Two-photon Laser-written Photoalignment Layers for Patterning Liquid Crystalline Conjugated Polymer Orientation

Yuping Shi, Patrick S. Salter,* Mo Li, Robert A. Taylor, Steve J. Elston, Stephen M. Morris,* and Donal D.C. Bradley**

Yuping Shi, Dr. Patrick S. Salter, Prof. Steve J. Elston, Prof. Stephen M. Morris
Department of Engineering Science, University of Oxford, Parks Road, Oxford, OX1 3PJ, UK
E-mail: yuping.shi@eng.ox.ac.uk; patrick.salter@eng.ox.ac.uk; stephen.morris@eng.ox.ac.uk

Dr. Mo Li, Prof. Robert A. Taylor, Prof. Donal D.C. Bradley
Department of Physics, University of Oxford, Parks Road, Oxford, OX1 3PU, UK

Prof. Donal D.C. Bradley
Physical Science and Engineering Division, King Abdullah University of Science and Technology, Thuwal, 23955-6900, Kingdom of Saudi Arabia
E-mail: donal.bradley@kaust.edu.sa

Keywords: liquid crystalline conjugated polymer, photoalignment, two-photon laser writing, polarized light emission, optical anisotropy

Systematic tuning of chemical and physical structure allows fine control over desired electronic and optical properties, including those of conjugated polymer semiconductors. In the case of physical structure, orientation via liquid crystalline alignment allows access to fundamental optical anisotropies and the associated refractive index modification offers great potential for fabrication of photonic structures. In this paper, photoalignment is used to orient the liquid crystalline conjugated polymer poly(9,9-dioctylfluorene-co-benzothiadiazole) (F8BT), specifically involving two-photon infrared laser writing of patterns in an azobenzene sulphonic dye (SD1). These patterns are transferred into the overlying film by thermotropic orientation in the nematic melt, then frozen in place by quenching to a room temperature nematic glass. Optimization of laser power and scan speed allows features with linewidths ≤ 1 μm. Photoluminescence (PL) peak anisotropy values reach $PL_{//} / PL_{\perp} = 13$ for laser writing, compared with $PL_{//} / PL_{\perp} = 9$ for polarized ultraviolet light emitting diode exposure of the same SD1 layer. These two approaches also result in different film microstructures; evidenced by characteristic changes in PL spectra. The anisotropic PL spectra provide information on

emissive excited states that complements previous studies on non-oriented F8BT and related copolymers, also suggesting two emissive states.

1. Introduction

For liquid crystalline conjugated polymers (LCCPs)[1-4] the performance of devices such as polarized light-emitting diodes,[5-10] microcavities,[11] lasers,[12-14] and field-effect transistors[7,15-17] depends keenly on the degree of alignment of the polymer chains. Orientational order reveals the fundamental anisotropy of the polymer chain in absorption and refractive index,[11,18,19] Raman scattering,[19,20] photoluminescence (PL),[5-10,21] stimulated emission[12-14] and charge carrier mobility.[7,15-17,22,23]

The long-range orientational order of a thermotropic nematic liquid crystal (LC) mesophase[24] is attractive in this regard but for LCCPs it is only entered at rather elevated temperatures (≈ 200 - 300 °C). The standard rubbed polyimide alignment layers used in the LC display industry are not normally stable in this range and bespoke high-temperature-stable polyimides or other polymers, such as poly(*p*-phenylenevinylene), have been used instead.[1,6,25] Furthermore, these alignment layers generally require a mechanical rubbing process that can introduce contaminants (abraded from the surface) and yield unwanted surface roughness, both of which are undesirable for device application. In addition, the absence of a ready means to spatially pattern the alignment layer makes the fabrication of photonic structures such as diffractive optical elements and waveguides highly challenging. This motivates the search for alternative non-mechanical alignment processes.[7]

Photoalignment layers offer a promising alternative to rubbed high-temperature polyimides, with previous studies demonstrating alignment of LCCPs for a range of device applications.[8,16,21,26-28] One such photoalignment layer, sulphonic azo-benzene dye (SD1), has

received considerable past attention for use in LC devices[29-31] as well as for indirect alignment of functional nanostructures.[32 - 36] Recently, SD1 has also been shown to be capable of orienting LCCPs such as poly(9,9-dioctylfluorene-co-benzothiadiazole) (F8BT) and other fluorene-based polymers, yielding optical anisotropies comparable to those observed using rubbed high-temperature polyimide alignment layers. [1,18,19,25,27,28]

While photoalignment layers such as SD1 are prone to photo- and environmental-instabilities,[24,30] this is not a limiting factor for their use in orienting LCCPs. In the polymer liquid crystalline phase, alignment is triggered by interface interactions between the polymer chain and the alignment layer which are then communicated through the bulk of the conjugated polymer film by chain-chain interactions. Upon rapid quenching to room temperature the long-range nematic orientation of the polymer chains is frozen into a nematic glass state that does not then require the photoalignment layer to maintain its order.

The use of photoalignment layers also presents a versatile means of patterning the LCCP orientation. Microscopic features can be formed by masking the exposure of the layer to polarized light as demonstrated by Zhang *et al.*[27] who reported linear and curvilinear LCCP orientation features with linewidths down to ≈ 3 μm. A maskless approach using laser writing in turn offers improved pattern resolution and a greater flexibility to reconfigure the pattern design by programming the laser or sample stage movements; such direct laser writing has been shown to be a powerful tool for producing high-resolution spatial-patterning in a number of functional optical materials.[37-41]

In this work, we use two-photon laser writing/rewriting of SD1 alignment layers to generate high-quality orientation patterns in light-emitting F8BT films with ≈ 1 μm spatial resolution. Noticeably higher anisotropies in optical absorption and PL emission are observed for F8BT

films oriented on laser-patterned than on UV-LED-patterned SD1. The F8BT films oriented on laser written SD1 alignment layers also show a different microstructure. The combination of SD1 photoalignment layers with laser writing/rewriting creates an exciting new platform for the fabrication of a range of LCCP photonic structures.

2. Results and Discussion

SD1 was spin-coated as an ultra-thin (~5 nm) photoalignment layer onto Spectrosil substrates (see Experimental Methods for further details). If not exposed to linearly polarized light (either from the UV light source or the laser writer), the films exhibited no evidence of long range orientational order, as identified by the lack of macroscopic ordering of the polymer chains in the F8BT polymer layer when coated on to unaligned SD1 and annealed. Illumination at λ = 365 nm, close to the absorption peak of SD1 (Figure S3), results in the long molecular axis orienting in the plane of the substrate along a direction that is orthogonal to the excitation polarization.[30] The photoalignment of SD1 films is a rewritable process, which can allow different alignment patterns to be written into the same layer. As we will show, it is possible to first align the SD1 using polarized UV light before realigning in certain areas of the film using the laser writing process.

In the present work, this novel combination of spatially uniform alignment using polarized UV-LED-illumination and spatially patterned micron-scale alignment using two-photon laser writing has been employed. The resulting SD1 alignment was then transferred to an alignment of the LCCP chains in an overlying F8BT film that was 165 ± 5 nm thick, which was thermotropically aligned via annealing within its nematic liquid crystalline mesophase before quenching into a nematic glass (**Figure 1**). Absorption spectra for F8BT films in both non-oriented (as-spin-coated) and a uniformly oriented nematic glass state are presented in Figure S4. In this case the dichroic ratio at the long wavelength (~ 450 nm) peak was found to be 12.6

± 0.3, corresponding to an order parameter of $S \approx 0.85$. It was also observed that the largest dichroic ratios were recorded for F8BT films with a layer thickness of 180 to 190 nm when aligned using SD1 layers that were processed using the same UV-illumination conditions. Writing the pattern on an aligned SD1 layer enhances contrast and reduces polydomain defects (*vide infra*) which is highly desirable for many device applications.

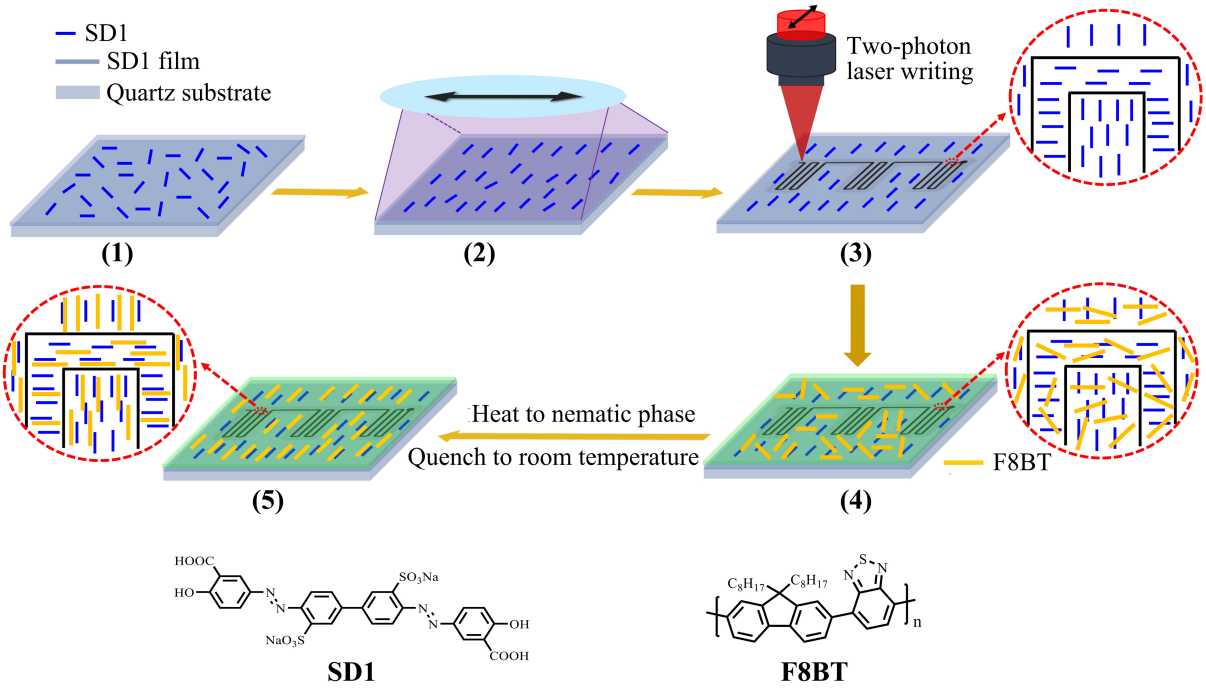

Figure 1. Schematic illustration of the procedure employed for the laser (re)writing of SD1 photoalignment layers to align F8BT LCCP films. (1) SD1 photoalignment layer is spin-coated onto a quartz substrate and (2) aligned initially through uniform exposure to linearly polarized UV illumination. (3) Regions of the photoalignment layer are then realigned using two-photon laser writing. The SD1 molecules orient perpendicular to the polarization of the incident light; here the reorientation is shown to be orthogonal to that of the UV-aligned background but it is possible to tune the relative angle by adjusting the laser beam polarization direction. An F8BT film is then spin-coated onto the SD1 layer (4) and heated to 265 °C (isotropic melt) before slow cooling into the nematic liquid crystal phase, where the polymer chains become oriented along a direction defined by the SD1 molecular orientation. The polymer chain and associated optical transition dipole moment orientations are then frozen-in by rapid quenching to room temperature (5) to form a nematic glass film. For direct two-photon laser writing the UV exposure alignment step is omitted leaving the SD1 background in a nonaligned state, which leads to no macroscopic alignment of F8BT across that region during subsequent thermal annealing.

Initially, linearly polarized UV light (λ = 365 nm) from an LED source was shone onto an SD1 film so as to initiate uniform alignment across the whole substrate. Subsequently, an

ultrafast Ti:sapphire laser source (λ = 785 nm) was tightly focused onto the SD1 layer so as to locally rewrite the alignment. The substrate was translated relative to the laser focus using an *x-y* stage, thereby writing an in-plane two-dimensional (2-D) alignment pattern (see Experimental Methods). Two-photon absorption, as a second order nonlinear optical process, depends on the square of the incident light intensity and is localized to within the focal region of the laser. This results in highly spatially localized cis-trans isomerization and reorientation of the SD1 molecules leading to micron- and sub-micron-scale patterning potential (*vide infra*). Adjusting the polarization direction of the writing laser (shown at 90° orientation in Figure 1) relative to that used to uniformly align the background using UV illumination, as well as controlling the beam spot size, laser power and scan speed allows generation of bespoke alignment patterns on-demand.

Separate tests with a conventional low molar mass nematic LC showed that the SD1 layer could be subjected to temperatures of up to 350 °C for at least 30 minutes after alignment without a significant degradation in the quality of the LC alignment, as determined by polarizing optical microscopy. Temperatures of 350 °C are generally significantly in excess of the clearing temperature for most LCCPs,[1,3,14,25,42] including the polyfuorene copolymer, F8BT, which is considered in this study. Orientation of F8BT was achieved by spin-coating the polymer onto the patterned SD1 alignment layer followed by an annealing process that was similar to that employed in previous studies;[19,25,28] this involved heating to above 265 °C and then slowly cooling to 247 °C. After holding at this temperature for 10 mins, the sample was then rapidly quenched to room temperature to avoid crystallization and freeze the liquid crystalline order into a nematic glass film.[1,14,20]

Polarized optical micrographs recorded with the samples placed between crossed polarizer and analyzer pairs reveal orientational order in the quenched nematic glass state resulting in

birefringence of the F8BT film. Micrographs are shown in **Figure 2** for differently patterned F8BT films; the images show three 100 μm × 100 μm squares (Figure 2a,b) and a crest pattern (Figure 2c,d). The excellent writability and rewritability of the SD1 photoalignment layer is clearly revealed. Both two-photon laser writing on nonaligned SD1 (squares) and two-photon laser rewriting on UV-aligned SD1 (crest pattern) are demonstrated. The images show a dark state when the chain orientation direction (defining the optic axis) is parallel to the transmission axis of either the polarizer or analyzer, resulting in no macroscopic birefringence. Conversely, when the orientation of the polymer chains is at 45° to the axes of the polarizer/analyzer then a high transmission state is observed. Monodomain F8BT orientation is observed in all of these images and can readily extend over cm^2 areas. A transition zone between the F8BT chains oriented on the UV-aligned SD1 background and those oriented on the laser rewritten SD1 crest pattern is clearly visible in Figure 2c,d and Figure S5. This region maps between two orthogonally oriented monodomain regions and as a consequence shows a texture that consists of defects in the F8BT alignment (*vide infra*). Examples of polarized optical micrographs and polarized PL intensity images for F8BT films oriented on crest patterns laser written into nonaligned SD1 are shown in Figure S6 where the resolution and contrast appear significantly reduced because, in this case, the background includes emission from polymer chains that randomly align with the polarization of the analyzer. Additional images for F8BT films oriented on crest patterns that were laser rewritten in UV-aligned SD1 backgrounds for different relative laser polarizations are shown in Figure S7.

Polarized PL intensity images for the square (Figure 2e,f) and crest (Figure 2g,h) patterns further emphasize the quality of the F8BT film orientation on the laser written (rewritten) alignment layers.

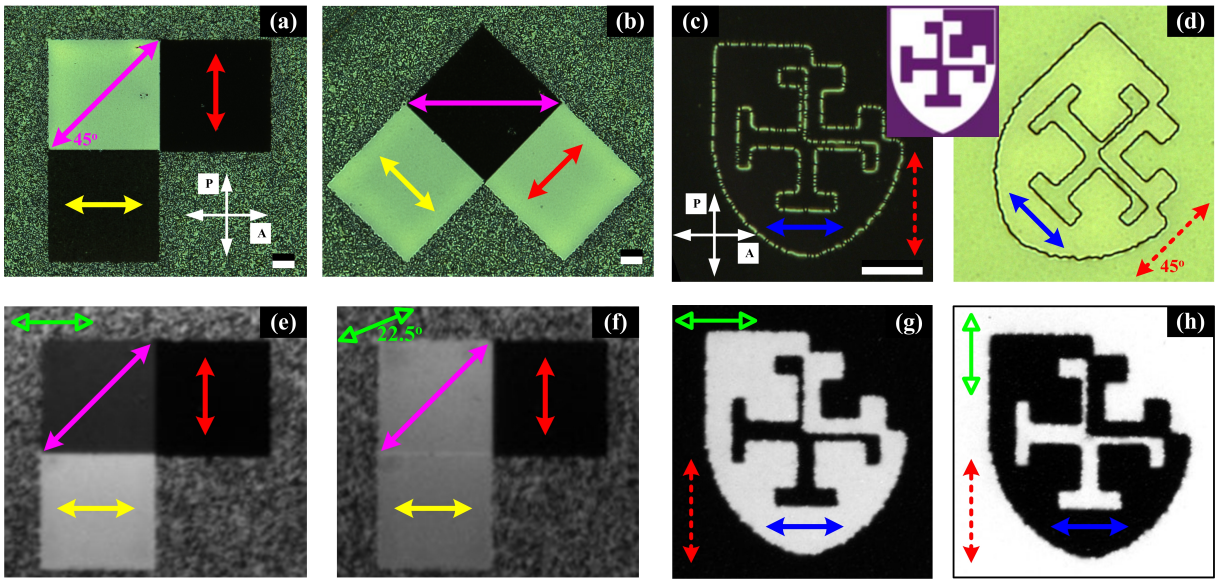

Figure 2. Polarized optical micrographs ((a), (b), (c), (d)) and polarized PL intensity images ((e), (f), (g), (h)) demonstrating laser patterned orientation in quenched nematic glass F8BT films. The micrographs are recorded with the samples placed between crossed polarizer and analyzer pairs; double headed white arrows in (a) and (c) delineate the polarization directions, labelled, respectively, P and A. The square patterns ((a) and (b)) were two-photon laser written with a bi-directional raster on a non-aligned SD1 layer using different optical polarizations and the F8BT films were then spin-coated on top before thermotropic alignment and quenching. The resulting F8BT chain axis orientation directions are indicated by double headed yellow, red and pink arrows for the three separate squares. The crest pattern ((c) and (d)) based on the St. Cross College Oxford crest (see inset) was laser rewritten on a UV-aligned SD1 film with a polarization direction at 90º relative to the UV-oriented background. The double headed blue and dashed red arrows show, respectively, the orientation of the polymer chains in the crest and the background. A dark state is observed when the orientation of the polymer chains is parallel to either the polarizer or analyzer whereas a bright state is observed when it is at 45° to axes of the polarizer/analyzer. For the crest, the visibility of the pattern only arises because of a transition region between the two orthogonal orientations which shows up bright for (c) and dark for (d), consistent with a local orientation that is intermediate between the two main orientations. Polarized PL intensity images are shown for the squares in (e) and (f) and the crest pattern in (g) and (h). Samples were excited at 450 nm with an unpolarized excitation source. The doubled headed green arrows show the orientation of the analyzer used to select the polarization of the collected emission light. There is clear correlation between the polarized PL intensity and the designed polymer chain alignment. The scale bars in all images are 20 μm.

In Figure 2e the squares show dark, intermediate and bright PL states for the analyzer polarization direction (indicated by the double-headed green arrow) that is orthogonal (double-headed red arrow), at 45° (double-headed pink arrow) and parallel (double-headed yellow arrow) to the orientation of the F8BT chain axis, respectively. In Figure 2f the analyzer is rotated by 22.5° whilst keeping the substrate orientation fixed. As a result, the angle of the

analyzer to the F8BT polymer chains in the squares (indicated by double-headed pink and yellow arrows) became 22.5° in both cases, thereby yielding the same relatively bright state, and 67.5° for the square indicated by the double-headed red arrow, yielding a relatively dark state. This demonstrates the possibility to create a grey scale in the PL intensity by tuning the chain orientation and the analyzer polarization directions. Figure 2g,h show the corresponding PL contrast for oriented F8BT on the laser rewritten crest pattern for the case where the analyzer and crest pattern orientations are parallel and orthogonal, respectively. In the parallel orientation case, the crest pattern PL is maximum (bright state) and in the orthogonal case minimum (dark state).

PL intensity maps of aligned F8BT films were also studied using polarized micro-PL (μ-PL) measurements (see Experimental Methods and Figure S2 in the Supplementary Information). Examples of such μ-PL maps are shown in **Figure 3a,b**, where the integrated spectral intensity is plotted both as a 2-D colour-coded image (bottom of Figure 3a & 3b) and a 3-D rendered image (top of Figure 3a & 3b) where zero PL intensity is located at the top of the *z*-axis and the intensity increases upon moving down the *z*-axis. These images were obtained with analyzer polarizations that are orthogonal to the direction of the F8BT chain orientation axis in the laser written crest. As a result, this arrangement results in a low intensity being recorded for the anisotropic emission from the crest and a higher intensity from the background.

In Figure 3a the crest pattern was laser written into an SD1 photoalignment layer that had already been prealigned using polarized UV illumination. The alignment of the chains in the crest was set to be at 90° relative to the UV-aligned background. In Figure 3b the SD1 layer was not aligned before laser writing the crest pattern. The results highlight the uniformity, especially for Figure 3a, in the patterned alignment over extended areas and the significant benefit in laser writing patterns into a uniformly aligned SD1 layer.

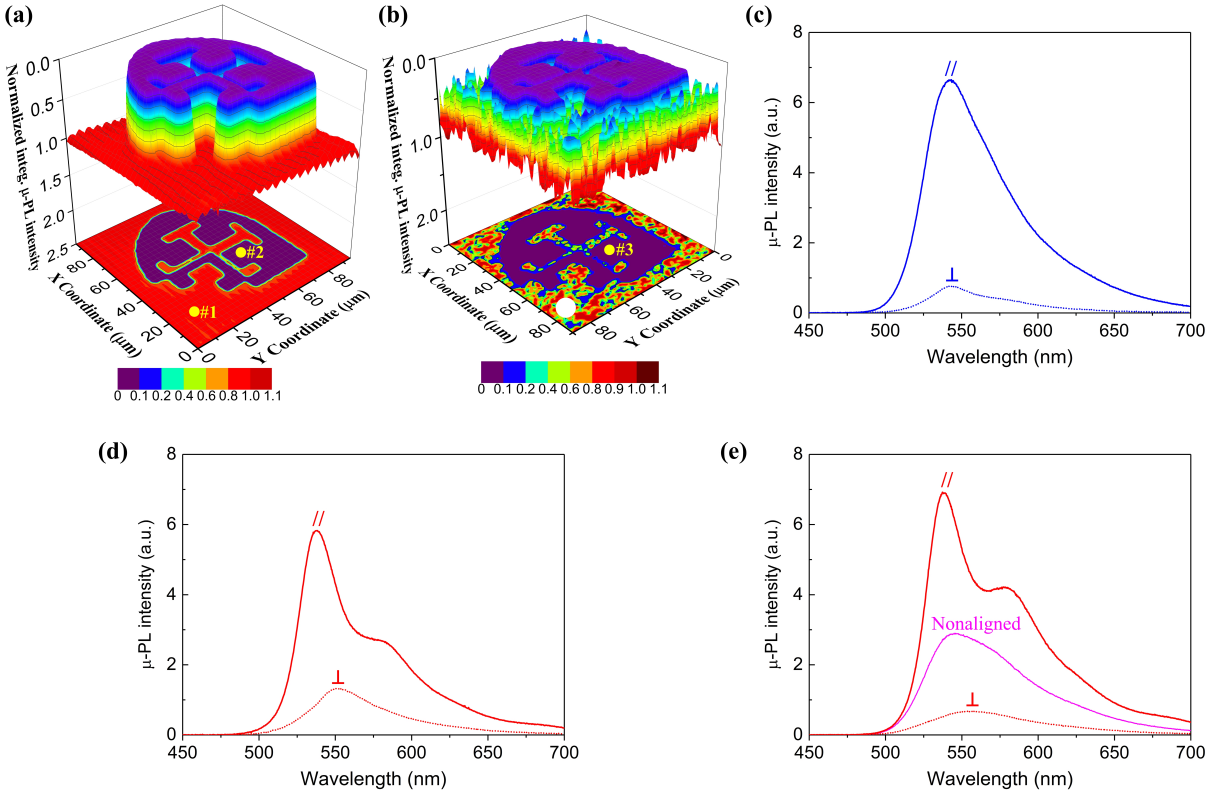

Figure 3. Spectrally integrated μ-PL intensity maps and selected spectra for different locations on F8BT films with laser (re)written SD1 alignment patterns. Intensity maps, where have been normalized to the maximum emission intensity in each case, are shown where the background was (a) aligned with UV illumination and (b) nonaligned. For (a), the excitation polarization and the PL collection polarization were aligned along the *x*-axis, which is orthogonal to the orientation of the F8BT polymer chains in the laser written crest and parallel to the UV-aligned background. For (b), the excitation was along the *y*-axis (chain alignment direction in the crest) and the PL collection polarization was along the *x*-axis. The small undulation in the intensity for the UV-aligned background is considered to be an experimental artefact. PL spectra are shown for: (c) location #1 in (a); (d) location #2 in (a); and (e) location #3 in (b) along with the spectrum from a nonaligned F8BT region highlighted by the white dot (bottom corner in the 2-D intensity map of (b)). For each location the excitation polarization was rotated to lie along the local chain orientation direction and PL spectra were collected with the analyzer both parallel and perpendicular to this direction. For the nonaligned spectrum, the excitation was along the *y*-axis and the analyzer polarization was along the *x*-axis.

The transition region noted in Figure 2 is also evident in the 2-D colour-coded image in Figure 3a in the form of an intermediate PL intensity lying more or less half way between the bright background and dark crest intensities. Figure 3c-e display the μ-PL spectra from different specific locations in Figure 3a and 3b, measured with a spot size of ≈ 1 μm diameter at the sample. In each case the 405 nm excitation source was polarized parallel to the local orientation

of the polymer chains and the emission from F8BT was separated using an analyzer to reveal the components polarized parallel ($PL_{//}$) and perpendicular ($PL_{\perp}$) to the chain orientation. Figure 3c shows the spectra recorded for F8BT oriented on a UV-aligned SD1 region that had not been subjected to laser rewriting (location #1, Figure 3a). From the spectra, the peak wavelengths for $PL_{//}$ and $PL_{\perp}$ occur at 543 ± 1 nm, with a weak shoulder at ~ 580 nm in the $PL_{\perp}$ spectrum. The PL anisotropy at 543 nm is found to be $PL_{//} / PL_{\perp} \approx 9$. This is consistent with results presented by Zhang *et al*.[27] The corresponding emission spectra recorded with excitation polarized perpendicular ($\perp$) to the polymer chains are shown in Figure S8a; no spectral differences are evident but, as expected, weaker emission results because of the weaker alignment between the excitation beam polarization and the absorption dipole moment orientation for F8BT; angle $\beta \approx 22°$ relative to the chain axis.[20]

The anisotropy in the PL emission spectra for an F8BT film that was aligned using the laser rewriting process on the UV-aligned SD1 background is shown in Figure 3d. In this case the excitation polarization was rotated to be aligned along the chain axis in the crest. The main peak at $\lambda = 538$ nm in $PL_{//}$ is at a slightly shorter wavelength than for the UV-aligned case ($\lambda = 544$ nm), whilst that for $PL_{\perp}$ (552 nm) is at a slightly longer wavelength (c.f. 543 nm). A second, weaker peak (at 580 nm) is also evident in $PL_{//}$. The PL anisotropy at the main $PL_{//}$ peak ($\lambda = 538$ nm) is found to be $PL_{//} / PL_{\perp} = 6.5$. The corresponding PL emission spectra recorded with excitation polarized perpendicular to the polymer chains are shown in Figure S8b; again, no spectral differences are evident and, as before, weaker emission results.

The polarized PL spectra in Figure 3e are for F8BT aligned on a crest region (location #3 in Figure 3b) that was laser written onto a nonaligned SD1 layer. They closely resemble the spectra shown in Figure 3d except that the emission anisotropy is larger and the peak at 580 nm

in $PL_{//}$ is more defined here. The PL anisotropy ratio at λ = 538 nm (parallel emission peak) is $PL_{//} / PL_{\perp} = 13$, which is notably bigger than recorded for the UV-aligned SD1 case (Figure 3c) and the laser rewritten crest in the UV-aligned background (Figure 3d). Values for the integrated PL anisotropy, on the other hand, are found to be $\int PL_{//} / \int PL_{\perp} = 10.1$, 8.4, and 4.1 for UV alignment, laser writing in a nonaligned background, and laser rewriting in a UV-aligned background, respectively. Also shown in Figure 3e is the nonaligned PL spectrum from an F8BT film following heating and quenching for a location atop a nonaligned SD1 layer; the spectrum peaks at 546 nm and generally matches PL spectra previously reported for nonaligned F8BT and other dialkylfluorene-benzothiadiazole containing conjugated molecules.[25,27,43,44]

Direct two-photon laser writing of the SD1 photoalignment layer thereby emerges as a promising method for the spatial patterning of oriented LCCP films. In addition, the alterations in the spectral characteristics point to a significant change in F8BT microstructure when oriented on laser written SD1 alignment layers. Assuming a single emission species with the different spectral features part of the same vibronic progression, the change between UV-exposed and laser written SD1 would be indicative of lower inhomogeneous broadening (increased resolution of the second peak) together with a smaller Huang-Rhys parameter (greater relative weight in the first (0-0) vibronic transition); the latter generally arises from a more rigid molecular geometry, potentially arising from chain extension during orientation.[45] This is not, however, in agreement with previous discussions of the PL spectral features in F8BT for which a model has been proposed that has two distinct emissive species, resulting from differing chain-packing motifs. The relative weighting of F8BT spectral components then depends on inter-chain, inter-BT unit contacts with an increase in direct BT to BT contact increasing the strength of the longer wavelength feature.[46] Further discussion on this point will follow below.

Comparing the cases when the laser writing is either into a nonaligned SD1 layer or one that has been aligned initially using UV illumination, we note that the smaller polarization ratio observed for the latter seems to signal a reduction in the overall degree of F8BT chain orientation atop the laser rewritten SD1 and/or an increase in the off-axis component of the corresponding transition dipole moment. The latter possibility can be investigated using a combination of absorption and Raman anisotropy measurements;[19,20] an interesting topic for future study. The combination of UV-alignment followed by two-photon laser writing will not cause any oxidative damage to the F8BT film as these steps are taken prior to coating the polymer film and performing a single thermal annealing cycle that is the same for all samples. It might be, however, that the SD1 layer is susceptible to photooxidative damage leading to a reduced ability to generate subsequent alignment of F8BT; a follow-up study is planned.

From the spectra in Figure 3, while also referring to Figure S9 which plots all spectra in a normalized peak intensity format for closer comparison, we can make some general observations. The PL emission from the F8BT layer atop a nonaligned SD1 layer is, as expected, independent of the analyzer orientation and similar to many published spectra for spin-coated F8BT films.[46] The emissive excited state is reported to have significant charge transfer character which will likely lead to shifts in spectral position dependent on packing density and local dielectric environment.[47]

The PL from the F8BT film on a UV-aligned SD1 layer (Figure S9, blue line) exhibits a narrower spectral linewidth than that from nonaligned films for both emission polarization components. In addition, the $PL_{\perp}$ emission spectrum for the F8BT on a UV-aligned SD1 layer shows resolution of a weak shoulder at 580 nm. The F8BT PL spectra from the laser-aligned SD1 on a UV-aligned background (Figure S9, red line) differs in that the resolution of a second

peak/shoulder at 580 nm appears in the $PL_{//}$ spectra (compared to the $PL_{\perp}$ component for the case of the UV-aligned sample), whereas, the $PL_{\perp}$ spectra is relatively featureless, peaking at ≈ 552 nm. The $PL_{//}$ spectrum for the laser-written crest in the nonaligned background (Figure S9, green line) is similar to that seen for the crest in the UV-aligned background (albeit with more definition in the peak/shoulder at 580 nm), the spectrum recorded for the $PL_{\perp}$ component is rather broader, although still relatively featureless.

Figure S10 shows normalized PL spectra for a F8BT film aligned on both a laser rewritten crest pattern on a UV aligned SD1 background (a) and the background (b); for excitation and emission light that is polarized parallel and perpendicular to the chain orientation. The spectra further highlight the differences in the PL emission between F8BT layers on laser (re)written and UV aligned SD1, with laser (re)written regions exhibiting more definition in the spectra with a clear secondary peak/shoulder at 580 nm as well as a noticeable red-shift in the spectrum for the $PL_{\perp}$ component. No such redshift is observed for the PL emission from the UV aligned regions and, furthermore, the weak appearance of a second peak at 580 nm is seen in the $PL_{\perp}$ not the $PL_{//}$ spectral component.

Taking all of the PL spectral information into account leads to the conclusions (i) that the resulting film microstructure is significantly dependent on how the SD1 layer is aligned, reflecting the different microstructuring and/or molecular alignment of SD1, which is a topic for more detailed investigation in further studies and (ii) that whilst the spectra do appear to have contributions from two emissive species, as reported in the literature,[43] these are not spectrally separated as previously assumed.

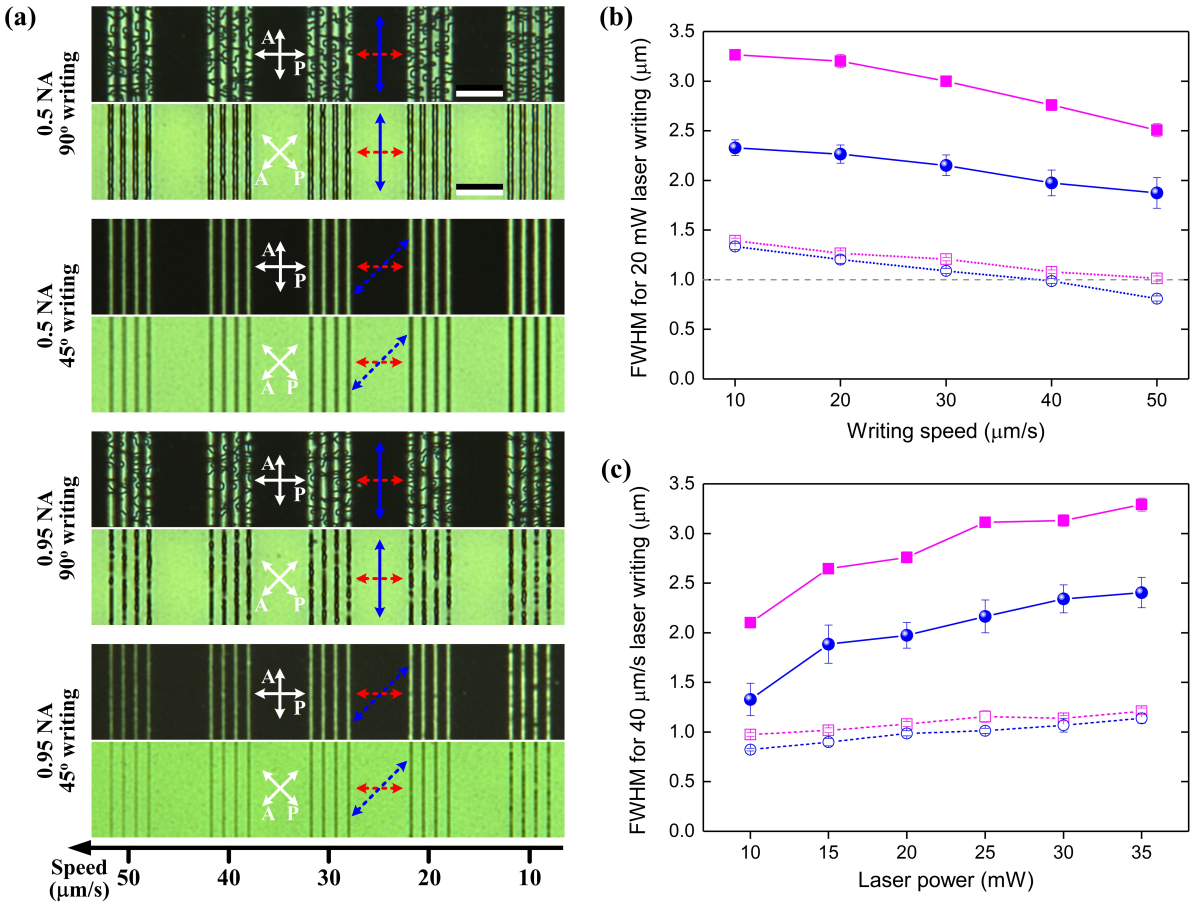

Figure 4. F8BT laser pattern resolution optimization. (a) Crossed-polarizer optical microscope images for F8BT oriented on groups of four laser rewritten SD1 lines at 5 μm separation intervals on a UV-aligned uniform SD1 background. Double headed white arrows represent the polarization directions for the incident light polarizer, P, and the transmitted light analyzer, A. The top two panes (each with dark and bright states for the background) were rewritten using the 0.5 NA and the bottom two the 0.95 NA objective lens. The writing (substrate displacement) speed used for each set of lines is shown as a graded scale at the bottom of the sub-figure. Results are presented for polarizations of the rewriting laser that are either at 90° (solid double headed blue arrow; 1st and 3rd panes) or 45° (dashed double-headed blue arrow; 2nd and 4th panes) relative to the uniform UV-aligned background (dashed double headed red arrows). These images were used to extract the FWHM linewidth of the patterned F8BT orientation stripes. The FWHM is plotted as a function of laser writing speed in (b) and laser power in (c), parametric in each case in the objective lens numerical aperture (NA = 0.5, red squares; 0.95, blue circles) and laser polarization relative to the background uniform UV-alignment polarization (90° writing, filled symbols; 45° writing, open symbols). The horizontal dash-dotted line in (b) delineates a 1μm FWHM.

What we observe, most clearly in Figure 3d (and Figure S8b), is that one species gives rise to a vibronically structured emission with clearly resolved 0-0 and 0-1 peaks at ~ 538 and ~ 580 nm (c.f. Figure 3d $PL_{//}$ spectrum) and the other species gives rise to an unstructured red-shifted

emission (c.f. Figure 3d $PL_{\perp}$ spectrum) peaking in this case at ~ 552 nm. The use of polarized detection helps to separate the two components and suggests that the second component may have a more inter-chain character. The literature explanation of two F8BT emissive states depending on the relative orientation of F8 and BT units in neighbouring chains does not fully align with these observations; if nothing else, the existence of vibronic structure has not been included within that description. The existence of two overlapping emission contributions makes analysis of anisotropies more difficult, especially since, as surmised here, it may be that one of the species has a more inter-chain, orthogonally polarized, character.

An advantage of the two-photon laser rewriting process is the potential for rapid prototyping of complex photonic structures at high resolution. Experiments were carried out to optimize the writing parameters and improve the patterning resolution and F8BT alignment quality. Laser patterning was performed on uniformly UV-prealigned SD1 layers for a range of writing powers and speeds (i.e. substrate displacement rates). Different focusing optics were also used, with 0.5 and 0.95 numerical aperture (NA) lenses yielding theoretically predicted focal spot sizes of 0.8 μm and 420 nm full width at half maximum (FWHM), respectively. Results are shown in **Figure 4** for two different orientations (90° and 45°) of the incident laser polarization with respect to the UV light polarization used for SD1 prealignment.

From inspection of Figure 4a, there is clearly a different microstructure for F8BT orientation on laser-rewritten SD1 stripes at 90° and 45° alignment relative to the background. The former shows distinct non-uniformity with clear Schlieren textures. Disclination lines are visible throughout the 90° rewriting features, as can also be seen at the border of the laser rewritten pattern in Figure 2c; these remain black between cross-polarizers for all azimuthal sample orientations. Such defects arise only for the 90° rewriting, since when the LCCP is heated into its nematic phase, there is degeneracy between the two possible orientations of the director at

the border of the laser rewritten SD1, leading to formation of $\lambda = ½$ disclinations. For the 45° rewriting, the degeneracy is lifted such that there is no defect formation, and uniform lines at higher resolution are achievable (see also laser written crest in Figure S6).

In terms of the limit of the laser-written width for the 90º orientation of the laser polarization relative to that for the polarised UV-aligned regions, there are three factors that should be considered: (i) the patterning resolution currently available for our two-photon laser writing setup is limited by the positioning resolution of our translation stage (~50 - 100 nm) and the diffraction limit ~300 nm; (ii) from a materials point of view, a limiting factor could be the contour length of the F8BT backbone, which is often determined to be 10 - 20 nm from grazing-incidence wide-angle X-ray scattering; and (iii) chain entanglement may also play an important role in essentially limiting the spatial patterning resolution that can be achieved in the quenched F8BT films.

Extraction of the greyscale line profiles for all of the laser-rewritten lines in Figure 4a and averaging over each set of four lines rewritten with the same parameters, yields the FWHM values that are plotted in Figures 4b and 4c as a function of, respectively, writing speed and laser power. Decreasing the laser power and increasing the writing speed is effective in reducing the linewidth of the reoriented F8BT lines. Whether this is due to secondary (scattered and/or reflected) light interactions with SD1 broadening the region exposed remains to be answered. Additionally, as expected, the patterning resolution is higher for lines patterned with a smaller laser spot size. The minimum FWHM linewidth was obtained using the 0.95 NA objective and writing with 45° relative polarization and was determined to be less than 1 μm. This linewidth is still somewhat larger than the theoretically predicted laser spot size (420 nm FWHM), which is possibly a consequence of the finite distance required for director reorientation in the nematic phase of the F8BT film, as dictated by the elasticity of the medium. The similarity between 0.5

NA and 0.95 NA in this regard also suggests an underlying limitation. It should be noted though that the extracted linewidth is close to the diffraction limited resolution of our cross-polarized optical microscope and, therefore, the actual linewidth may indeed be lower than the ≈ 1 μm value determined here. We will seek in future to deploy higher resolution instruments such as polarized scanning transmission X-ray microscopy[48] or scanning nanodiffraction in transmission electron microscopy.[49] Irrespective, the resolution limit demonstrated here is still substantially smaller than that reported recently using non-laser-based, photomasked UV alignment.[27]

3. Summary and conclusions

In summary, a method for creating patterned structures in liquid crystalline conjugated polymers (LCCP) has been proposed and demonstrated using a combination of laser writing and the photoalignment material SD1. The laser writing process has the potential to create photonic structures with large PL anisotropies and high-quality alignment that could boost the optoelectronic performance more generally for devices such as polarized polymer light-emitting diodes, microcavity lasers and polymer field effect transistors. This method may also promote the development of more sophisticated photonic devices that make full use of the polarization degrees of freedom for PL excitation and detection, together with multi-level writing of spatial features oriented at different degrees relative to each other.

In particular, we have used two-photon laser writing with an ultrafast Ti:sapphire laser (785 nm, 250 fs, 80 MHz). The sample is scanned relative to the focused laser beam allowing sub-micron lateral resolution for suitably optimised writing conditions: laser power ~ 10 - 20 mW and scanning speed ~ 40 - 50 μm / s. Spatial patterrning can either be performed by laser writing

on an unexposed SD1 film or rewriting on an SD1 film pre-aligned by uniform UV diode exposure. Higher contrast is achieved for integrated PL images when laser rewriting is used as the ordering of the background produces a highly uniform (monodomain) signal against which the pattern more clearly stands out. UV alignment and laser (re)writing produce different F8BT film microstructures as judged by PL spectral differences and additional studies will he needed to fully interpret these differences.

Rewriting can be done using a range of different relative angles between the pre-alignment direction and the laser-writing polarization. When the laser polarization is selected to be orthogonal to the UV pre-alignment direction there is a well-defined transition zone between the monodomains (Figure 2). This transition zone displays clear Schlieren textures with $\lambda = ½$ disclination defects. For 35° and 45° rewriting, however, the director degeneracy that causes this transition zone is lifted and there is no defect formation (Figure S7 and Figure 4). The transition zone has a finite width that limits the linewidth resolution for 90° rewriting. As a consequence, 45° rewriting consistently gives narrower lines (Figure 4) for a variety of writing parameters.

Topics for further study include: (i) A more detailed exploration of the limiting factors for PL anisotropy in relation to the F8BT microstructure and the associated optical transition dipole moment orientation relative to the chain axis director. Absorption dichroism and Raman anisotropy measurements will allow the transition dipole moment orientation to be deduced independently of the PL measurements and the microstructure can be probed using X-ray and electron diffraction together with direct electron microscopy imaging techniques. (ii) Probing the rewriting process and the formation of disclination defects at the boundary between orthogonal monodomains using high resolution imaging techniques. (iii) Investigating the use

of laser written alignment in the fabrication of devices such as polarized polymer light-emitting diodes, microcavity lasers and polymer field effect transistors.

4. Experimental Methods

Materials and Film Preparation: The photo-alignment layer material, SD1, was provided by DIC Corporation Japan and used as received. The F8BT LCCP with average molecular weight, M_w = 55,000 and polydispersity index, PDI = 2.3 was purchased from 1-Material and also used as received. The photoalignment layers were spin-coated from 1 mg/ml SD1 solutions in anhydrous 2-methoxyethanol (≥ 99.8%) onto pre-cleaned polished Spectrosil substrates at 500 rpm for 5 seconds then 2000 rpm for 20 seconds. Samples were annealed at 110 °C for 10 minutes in ambient conditions to ensure solvent removal and alignment was then performed via uniform polarized UV light exposure or laser patterning as described below. F8BT was spin-coated onto uniform or patterned SD1 alignment layers from 30 mg/ml solutions in anhydrous toluene (99.8%) at 1750 rpm for 45 seconds. The F8BT films were vacuum-dried for >1 hour to remove excess solvent and then subjected to thermotropic alignment as described below.

UV Alignment of SD1 Layers: SD1 layers were aligned by irradiating the samples in air with 5 mW/cm^2 linearly polarized 365 nm light from a Thorlabs CS2010 UV-curing LED system equipped with a WP25M-UB broadband wire-grid polarizer. Prior to spin-coating F8BT films on top, the aligned SD1 layers were heated at 110 ^{o}C in air for 10 mins to thoroughly dry.

Two-photon Laser (re)writing of the SD1 Photoalignment Layers (c.f. Figure S1): The ultrafast Ti:sapphire laser used for two-photon alignment of SD1 was a 250 fs pulse duration, 785 nm central wavelength, 80 MHz repetition frequency, Spectra Physics Mai Tai oscillator. The laser was linearly polarized, using a half waveplate to adjust the polarization direction and a reflective variable neutral density wheel to adjust the power. The beam from the laser was

expanded to fill the pupil of a high numerical aperture (NA) microscope objective lens (Zeiss 20×, 0.5 NA or Olympus 50×, 0.95 NA). The SD1 sample for photoalignment was mounted (in air) on a high-precision (± 50 nm *x*-*y* repeatability), 3-D positioning stage comprising linked Aerotech ABL10100 (*x*-*y*) and ANT-95 (*z*) stages. Translation of the substrate relative to the fixed laser focus allowed the desired alignment patterns to be written. The average laser power used for photoalignment was measured using a thermal power meter placed just before the objective lens. Two-photon laser patterning was done both by writing on non-aligned SD1 layers and by rewriting on SD1 previously uniformly aligned using UV light.

Alignment of the F8BT Films Using UV- or two-photon Laser-aligned SD1 Layers: Thermotropic mesophase alignment of F8BT films spin-coated on top of patterned SD1 alignment layers was carried out using a Linkam THMS600 hotstage. The sample was heated at 20 °C /min to 265 °C (melt) before being slowly cooled at 3 °C / min to 247 °C (nematic phase) and held there for 10 mins. The sample was then rapidly quenched to room temperature by transferring the sample from the hotstage onto a copper bar. This quenching step prevents crystallization and thereby "freezes-in" the SD1 mediated ordering of the F8BT polymer chains, yielding a highly oriented nematic glass. All steps were carried out in a nitrogen atmosphere glovebox operated with < 1 ppm moisture and oxygen content. F8BT film thicknesses were measured using a Dektak profilometer.

Polarized UV-vis Absorption and Polarized Micro-PL Characterisation: Polarized UV-vis absorption spectroscopy was carried out using a PerkinElmer Lambda 1050. For this study a Glan-Thompson polarizer was mounted in front of the F8BT films to generate a linearly polarized incident beam. The relative orientation of the polymer chains to this incident light polarization was then varied by rotating the F8BT film in the vertical plane on a rotation stage. Micro-PL spectra were recorded at room temperature with linearly polarized 405 nm, 150 fs,

76 MHz excitation from a frequency doubled Ti:sapphire laser, using the schematic setup shown in Figure S2. The spot size at the sample was ≈ 1 μm diameter.

Supporting Information

Supporting Information is available from the Wiley Online Library or from the author.

Acknowledgements

YS and DDCB gratefully acknowledge the Hong Kong Jockey Club Graduate Scholarship at the University of Oxford for financial support. PSS gratefully acknowledges funding from the Engineering and Physical Sciences Research Council UK (EP/R004803/1). The authors collectively thank Dr. Ian Dobbie and the Micron Centre for Advanced Bioimaging in the Department of Biochemistry at the University of Oxford for help to obtain the polarized fluorescence images in Figure 2. YS thanks Professor Paul Stavrinou for useful discussions regarding polarized UV-vis absorption spectrocopy. DDCB thanks Dr Hiroshi Hasebe and DIC Corporation Japan for providing the SD1 photoalignment layer material used in these experiments and Professor Hoi Sing Kwok for facilitating the interaction. DDCB further thanks the Jiangsu Industrial Technology Research Institute - Oxford University Innovative Materials for Advanced and Critical Technologies (JITRI-Oxford IMPACT) Institute for partial support.

References

[1] M. Grell, D. C. C. Bradley, M. Inbasekaran, E. P. A. Woo, *Adv. Mater.* **1997**, 9, 798.

[2] M. Grell, D. D. C. Bradley, X. Long, T. Chamberlain, M. Inbasekaran, E. P. Woo, M. Soliman, *Acta Polymerica* **1998**, 49, 439.

[3] M. Grell, D. D. C. Bradley, *Adv. Mater.* **1999**, 11, 895.

[4] M. Grell, D. D. C. Bradley, G. Ungar, J. Hill, K. Whitehead, *Macromol.* **1999**, 32, 5810.

[5] M. Grell, W. Knoll, D. Lupo, A. Meisel, T. Miteva, D. Neher, H. G. Nothofer, U. Scherf, A. Yasuda, *Adv. Mater.* **1999**, 11, 671.

[6] K. S. Whitehead, M. Grell, D. D. C. Bradley, M. Jandke, P. Strohriegl, *Appl. Phys. Lett.* **2000**, 76, 2946.

[7] Z. Zheng, K. H. Yim, M. S. M. Saifullah, M. E. Welland, R. H. Friend, J. S. Kim, W. T. S Huck, *Nano Lett.* **2007**, 7, 987.

[8] K. Sakamoto, K. Miki, M. Misaki, K. Sakaguchi, M. Chikamatsu, R. Azumi, *Appl. Phys. Lett.* **2007**, 91, 183509.

[9] M. Misaki, M. Chikamatsu, Y. Yoshida, R. Azumi, N. Tanigaki, K. Yase, S. Nagamatsu, Y. Ueda, *Appl. Phys. Lett.* **2008**, 93, 023304.

[10] G. J. Choi, Q. V. Le, K. S. Choi, K. C. Kwon, H. W. Jang, J. S. Gwag, S. Y. Kim, *Adv. Mater.* **2017**, 29, 1702598.

[11] T. Virgili, D. G. Lidzey, M. Grell, S. Walker, A. Asimakis, D. D. C. Bradley, *Chem. Phys. Lett.* **2001**, 341, 219.

[12] T. Virgili, D. G. Lidzey, M. Grell, D. D. C. Bradley, S. Stagira, M. Zavelani-Rossi, S. De Slivestri, *Appl. Phys. Lett.* **2002**, 80, 4088.

[13] G. Heliotis, R. Xia, K. S. Whitehead, G.A. Turnbull, I. D. W. Samuel, D. D. C. Bradley, *Synth. Met.* **2003**, 139, 727.

[14] R. Xia, M. Campoy-Quiles, G. Heliotis, P. Stavrinou, K.S. Whitehead, D. D. C. Bradley, *Synth. Met.* **2005**, 155, 274.

[15] H. Sirringhaus, R. J. Wilson, R. H. Friend, M. Inbasekaran, W. Wu, E. P. Woo, M. Grell, D. D. C. Bradley, *Appl. Phys. Lett.* **2000**, 77, 406.

[16] K. Sakamoto, T. Yasuda, K. Miki, M. Chikamatsu, R. Azumi, *J. Appl. Phys.* **2011**, 109, 013702

[17] T. Endo, T. Nagase, T. Kobayashi, H. Naito, *Jpn. J. Appl. Phys.*, **2013**, 52, 121601.

[18] M. Campoy-Quiles, P. G. Etchegoin, D. D. C. Bradley, *Phys. Rev. B* **2005**, 72, 045209.

[19] M. C. Gather, D. D. C. Bradley, *Adv. Funct. Mater.* **2007**, 17, 479.

[20] H. M. Liem, P. Etchegoin, K.S. Whitehead, D. D. C. Bradley, *Adv. Funct. Mater.* **2003**, 13, 66.

[21] K. Sakamoto, K. Usami, Y. Uehara, U. Sukekatsu, *Appl. Phys. Lett.* 87, **2005**, 211910.

[22] M. Redecker, D. D. C. Bradley, M. Inbasekaran, E. P. Woo, *Appl. Phys. Lett.* **1999**, 74, 1400.

[23] R. Noriega, J. Rivnay, K. Vandewal, F. P. V. Koch, N. Stingelin, P. Smith, M. F. Toney, A. A. Salleo, *Nat. Mater.* **2013**, 12, 1038.

[24] A. M. Donald, A. H. Windle, *Liquid Crystalline Polymers*, Cambridge University Press, Cambridge, **1992**.

[25] M. Grell, M. Redecker, K. Whitehead, D. D. C. Bradley, M. Inbasekaran, E.P. Woo, *Liquid Crystals* **1999**, 26, 1403.

[26] D. Sainova, A. Zen, H. G. Nothofer, U. Asawapirom, U. Scherf, R. Hagen, T. Bieringer, S. Kostromine, D. Neher, *Adv. Funct. Mater.* **2002**, 12, 49.

[27] H. Zhang, L. Ma, Q. Zhang, Y. Shi, Y. Fang, R. Xia, W. Hu, D. D. C. Bradley, *Adv. Optical Mater.* **2020**, 1901958.

[28] F. Le Roux, R.A. Taylor, D. D. C. Bradley, *ACS Photonics* **2020**, 7, 746.

[29] K. Ichimura, *Chem. Rev.* **2000**, 100, 1847.

[30] V. G. Chigrinov, V. M. Kozenkov, H. S. Kwok, *Photoalignment of Liquid Crystalline Materials: Physics and Applications*, John Wiley & Sons, West Sussex, England, **2008**.

[31] O. Yaroshchuk, Y. Reznikov, *J. Mater. Chem.* **2012**, 22, 286.

[32] J. Schneider, W. Zhang, A. K. Srivastava, V. G. Chigrinov, H. S. Kwok, A. L. Rogach, *Nano Lett.* **2017**, 17, 3133.

[33] T. Seki, S. Nagano, M. Hara, *Polymer* **2013**, 54, 6053.

[34] E. A. Shteyner, A. K. Srivastava, V. G. Chigrinov, H.-S. Kwok, A. D. Afanasyev, *Soft Matter* **2013**, 9, 5160

[35] A. K. Srivastava, W. Zhang, J. Schneider, A. L. Rogach, V. G. Chigrinov, H.-S. Kwok, *Adv. Mater.* **2017**, 29, 1701091.

[36] T. Du, J. Schneider, A. K. Srivastava, A. S. Susha, V. G. Chigrinov, H. S. Kwok, A. L. Rogach, *ACS Nano* **2015**, 9, 11, 11049

[37] C. C. Tartan, J. Sandford O'Neill, P. S. Salter, J. Aplinc, M. J. Booth, M. Ravnik, S. M. Morris, S. J. Elston, *Adv. Optical Mater.* **2018**, 6, 1800515.

[38] G. Stoychev, A. Kirillova, L. Ionov, *Adv. Optical Mater.* **2019**, 1900067.

[39] C.A. Spiegel, M. Hippler, A. Münchinger, M. Bastmeyer, C. Barne-Kowollik, M. Wegener, E. Blasco, *Adv. Funct. Mater.* **2019**, 1907615.

[40] T. Gissibl, S. Thiele, A. Herkommer, H. Giessen, *Nat. Photonics* **2016**, 10, 554.

[41] A. Courvoisier, M. J. Booth, P. S. Salter, *Appl. Phys. Lett.* **2016**, 109, 031109.

[42] E. Lim, B. J. Jung, J. Lee, H. K. Shim, J. I. Lee, Y. S. Yang, L. M. Do, *Macromolecules* **2005**, 38, 4531.

[43] R.B. Fletcher, D.G. Lidzey, D. D. C. Bradley, M. Bernius, S. Walker. *Appl. Phys. Lett.* **2000**, 77 1262.

[44] C. R. Belton, A. L. Kanibolotsky, J. Kirkpatrick, C. Orofino, S. E. T. Elmasly, P. N. Stavrinou, P. J. Skabara, D. D. C. Bradley, *Adv. Funct. Mater.* **2013**, 23, 2792.

[45] M. Ariu, M. Sims, M. D. Rahn, J. Hill, A. M. Fox, D. G. Lidzey, M. Oda, J. Cabanillas-Gonzalez, D. D. C. Bradley, *Phys. Rev. B* **2003**, 67, 195333.

[46] C.L. Donley, J. Zaumseil, J.W. Andreasen, M. M. Nielsen, H. Sirringhaus, R. H. Friend, J. S. Kim, *J. Am. Chem. Soc.* **2005**, 127, 12890.

[47] J. M. Winfield, A. Van Vooren, M. J. Park, D. H. Hwang, J. Cornil, J. S. Kim, R. H. Friend, *J. Chem. Phys.* **2009**, 131, 035104.

[48] B. A. Collins, J. E. Cochran, H. Yan, E. Gann, C. Hub, R. Fink, C. Wang, T. Schuettfort, C. R. McNeill, M. L. Chabinyc, H. Ade, *Nat. Mater.* **2012**, 11, 536.

[49] C. J. Takacs, N. D. Treat, S. Krämer, Z. Chen, A. Facchetti, M. L. Chabinyc, A. J. Heeger, *Nano Lett.* **2013**, 13, 2522.

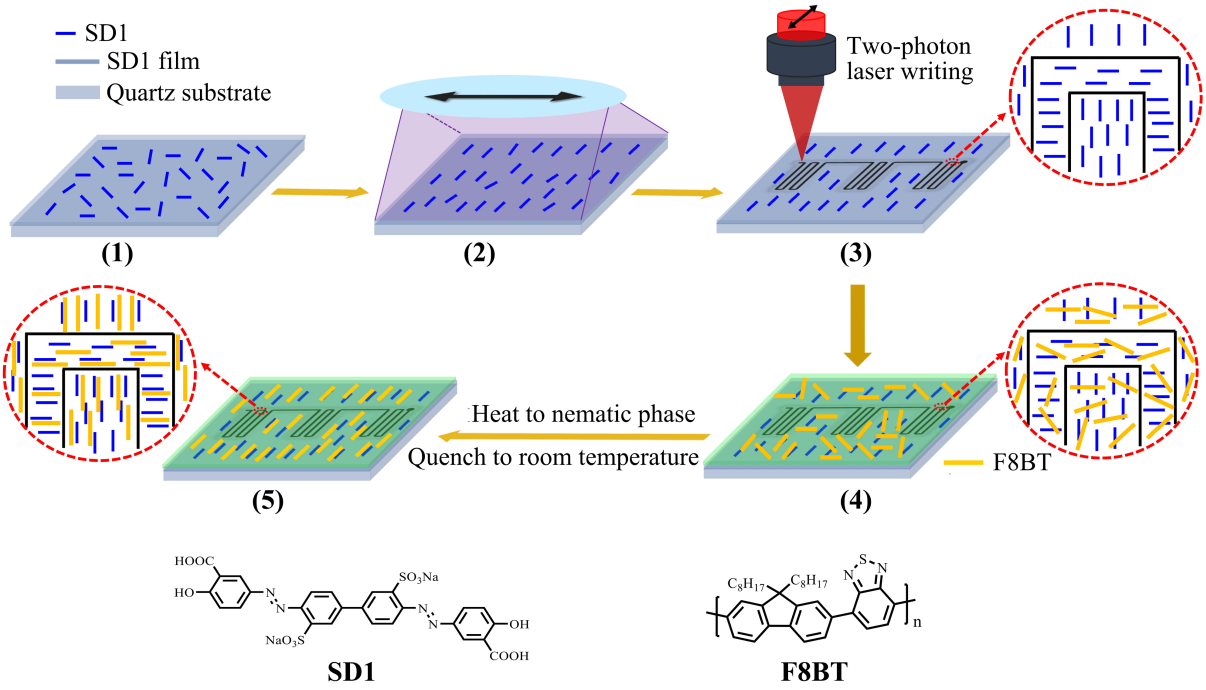

Figure 1. Schematic illustration of the procedure employed for the laser (re)writing of SD1 photoalignment layers to align F8BT LCCP films. (1) SD1 photoalignment layer is spin-coated onto a quartz substrate and (2) aligned initially through uniform exposure to linearly polarized UV illumination. (3) Regions of the photoalignment layer are then realigned using two-photon laser writing. The SD1 molecules orient perpendicular to the polarization of the incident light; here the reorientation is shown to be orthogonal to that of the UV-aligned background but it is possible to tune the relative angle by adjusting the laser beam polarization direction. An F8BT film is then spin-coated onto the SD1 layer (4) and heated to 265 °C (isotropic melt) before slow cooling into the nematic liquid crystal phase, where the polymer chains become oriented along a direction defined by the SD1 molecular orientation. The polymer chain and associated optical transition dipole moment orientations are then frozen-in by rapid quenching to room temperature (5) to form a nematic glass film. For direct two-photon laser writing the UV exposure alignment step is omitted leaving the SD1 background in a nonaligned state, which leads to no macroscopic alignment of F8BT across that region during subsequent thermal annealing.

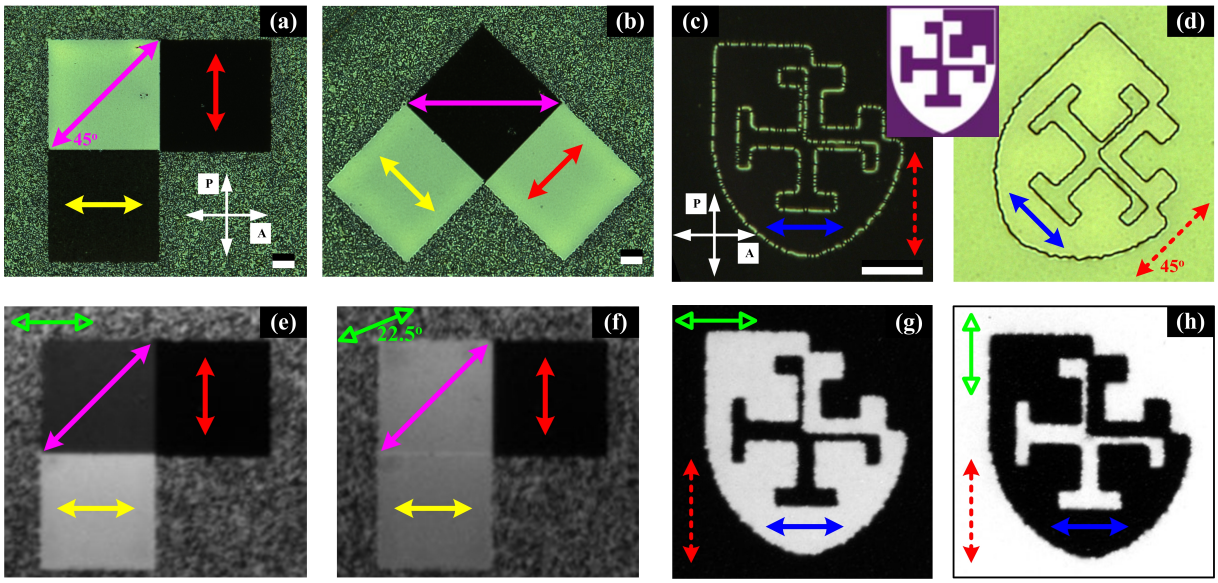

Figure 2. Polarized optical micrographs ((a), (b), (c), (d)) and polarized PL intensity images ((e), (f), (g), (h)) demonstrating laser patterned orientation in quenched nematic glass F8BT films. The micrographs are recorded with the samples placed between crossed polarizer and analyzer pairs; double headed white arrows in (a) and (c) delineate the polarization directions, labelled, respectively, P and A. The square patterns ((a) and (b)) were two-photon laser written with a bi-directional raster on a non-aligned SD1 layer using different optical polarizations and the F8BT films were then spin-coated on top before thermotropic alignment and quenching. The resulting F8BT chain axis orientation directions are indicated by double headed yellow, red and pink arrows for the three separate squares. The crest pattern ((c) and (d)) based on the St. Cross College Oxford crest (see inset) was laser rewritten on a UV-aligned SD1 film with a polarization direction at 90º relative to the UV-oriented background. The double headed blue and dashed red arrows show, respectively, the orientation of the polymer chains in the crest and the background. A dark state is observed when the orientation of the polymer chains is parallel to either the polarizer or analyzer whereas a bright state is observed when it is at 45° to axes of the polarizer/analyzer. For the crest, the visibility of the pattern only arises because of a transition region between the two orthogonal orientations which shows up bright for (c) and dark for (d), consistent with a local orientation that is intermediate between the two main orientations. Polarized PL intensity images are shown for the squares in (e) and (f) and the crest pattern in (g) and (h). Samples were excited at 450 nm with an unpolarized excitation source. The doubled headed green arrows show the orientation of the analyzer used to select the polarization of the collected emission light. There is clear correlation between the polarized PL intensity and the designed polymer chain alignment. The scale bars in all images are 20 μm.

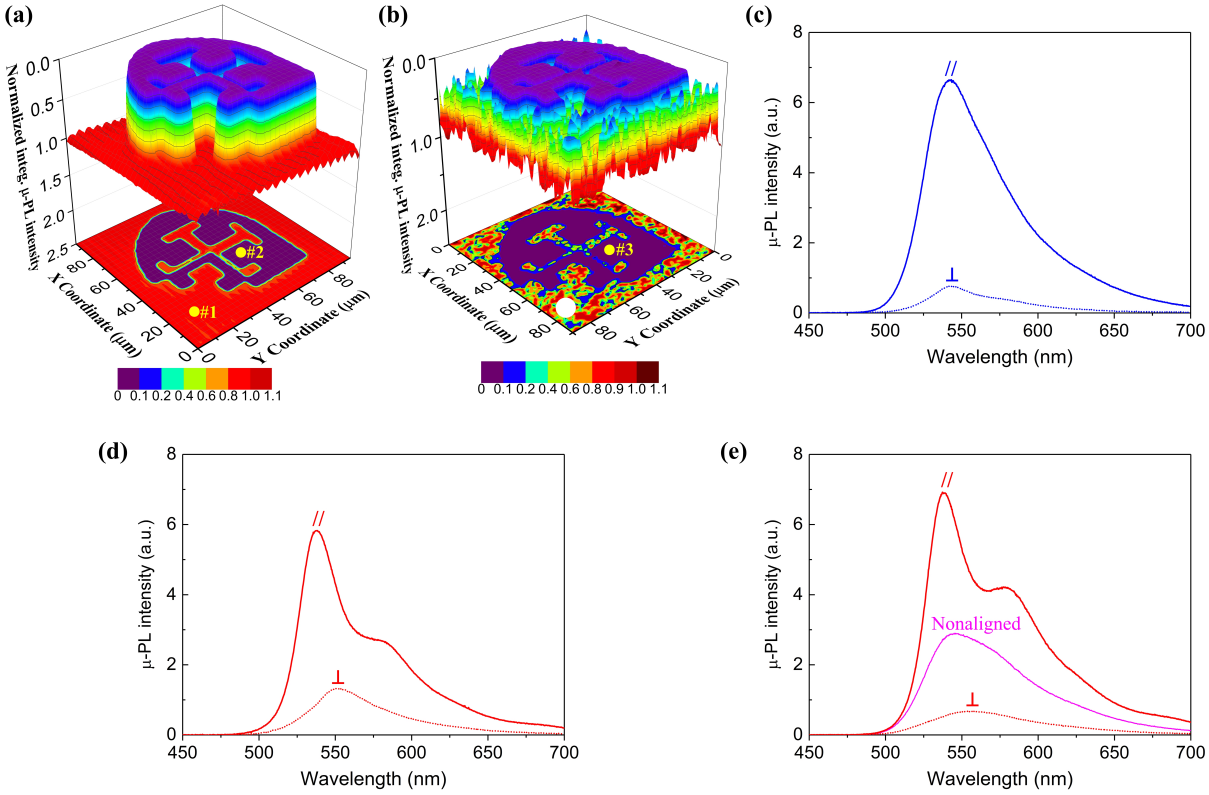

Figure 3. Spectrally integrated μ-PL intensity maps and selected spectra for different locations on F8BT films with laser (re)written SD1 alignment patterns. Intensity maps, where have been normalized to the maximum emission intensity in each case, are shown where the background was (a) aligned with UV illumination and (b) nonaligned. For (a), the excitation polarization and the PL collection polarization were aligned along the *x*-axis, which is orthogonal to the orientation of the F8BT polymer chains in the laser written crest and parallel to the UV-aligned background. For (b), the excitation was along the *y*-axis (chain alignment direction in the crest) and the PL collection polarization was along the *x*-axis. The small undulation in the intensity for the UV-aligned background is considered to be an experimental artefact. PL spectra are shown for: (c) location #1 in (a); (d) location #2 in (a); and (e) location #3 in (b) along with the spectrum from a nonaligned F8BT region highlighted by the white dot (bottom corner in the 2-D intensity map of (b)). For each location the excitation polarization was rotated to lie along the local chain orientation direction and PL spectra were collected with the analyzer both parallel and perpendicular to this direction. For the nonaligned spectrum, the excitation was along the *y*-axis and the analyzer polarization was along the *x*-axis.

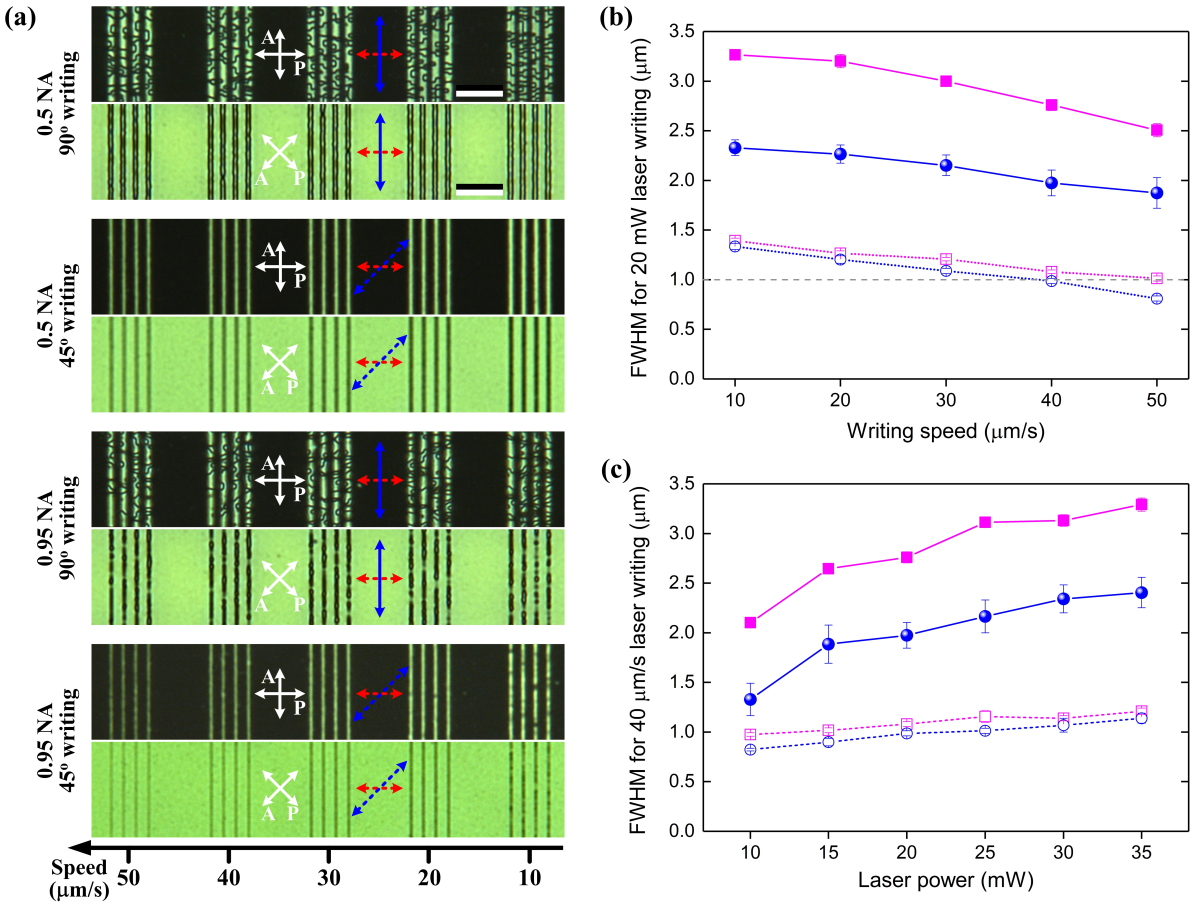

Figure 4. F8BT laser pattern resolution optimization. (a) Crossed-polarizer optical microscope images for F8BT oriented on groups of four laser rewritten SD1 lines at 5 μm separation intervals on a UV-aligned uniform SD1 background. Double headed white arrows represent the polarization directions for the incident light polarizer, P, and the transmitted light analyzer, A. The top two panes (each with dark and bright states for the background) were rewritten using the 0.5 NA and the bottom two the 0.95 NA objective lens. The writing (substrate displacement) speed used for each set of lines is shown as a graded scale at the bottom of the sub-figure. Results are presented for polarizations of the rewriting laser that are either at 90° (solid double headed blue arrow; 1st and 3rd panes) or 45° (dashed double-headed blue arrow; 2nd and 4th panes) relative to the uniform UV-aligned background (dashed double headed red arrows). These images were used to extract the FWHM linewidth of the patterned F8BT orientation stripes. The FWHM is plotted as a function of laser writing speed in (b) and laser power in (c), parametric in each case in the objective lens numerical aperture (NA = 0.5, red squares; 0.95, blue circles) and laser polarization relative to the background uniform UV-alignment polarization (90° writing, filled symbols; 45° writing, open symbols). The horizontal dash-dotted line in (b) delineates a 1μm FWHM.

Supporting Information

Two-photon Laser-written Photoalignment Layers for Patterning Liquid Crystalline Conjugated Polymer Orientation

Yuping Shi, Patrick S. Salter,* Mo Li, Robert A. Taylor, Steve J. Elston, Stephen M. Morris,* and Donal D.C. Bradley**

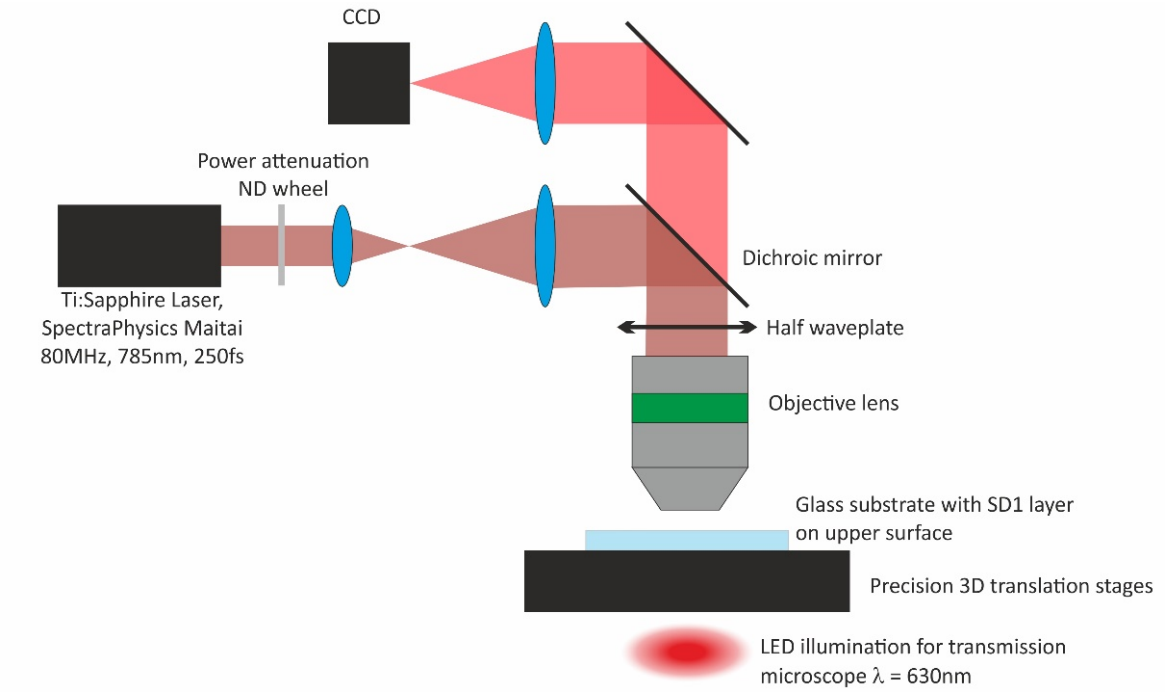

Figure S1: Experimental set-up for laser writing of the SD1 photoalignment layers. The laser source was a titanium sapphire ultrafast oscillator (Spectra Physics Maitai) with a central wavelength of 785 nm and a pulse repetition rate of 80 MHz. The pulse duration at the sample was 250fs. The laser was linearly polarized and the power was attenuated via a reflective variable neutral density (ND) wheel. The beam from the laser was expanded to fill the back aperture of a high numerical aperture microscope objective lens (Zeiss 20× 0.5NA or Olympus 50× 0.95NA). The SD1 sample for photoalignment was mounted beneath the objective lens on a 3D stack of high precision positioning stages (Aerotech ABL10100 (*x*-*y*) and ANT-95 (*z*)). The desired alignment patterns were written via translation of the substrate relative to the fixed laser focus. A rotatable half waveplate was positioned above the objective lens to control the direction of polarization on the sample, and hence the alignment direction of the SD1 layer. An LED (λ = 630nm) positioned beneath the sample provided illumination for a transmission microscope for real time monitoring of the sample during photoalignment. A dichroic mirror above the objective lens separated the light from the laser and the LED, with the LED light directed through a tube lens and onto a CCD detector.

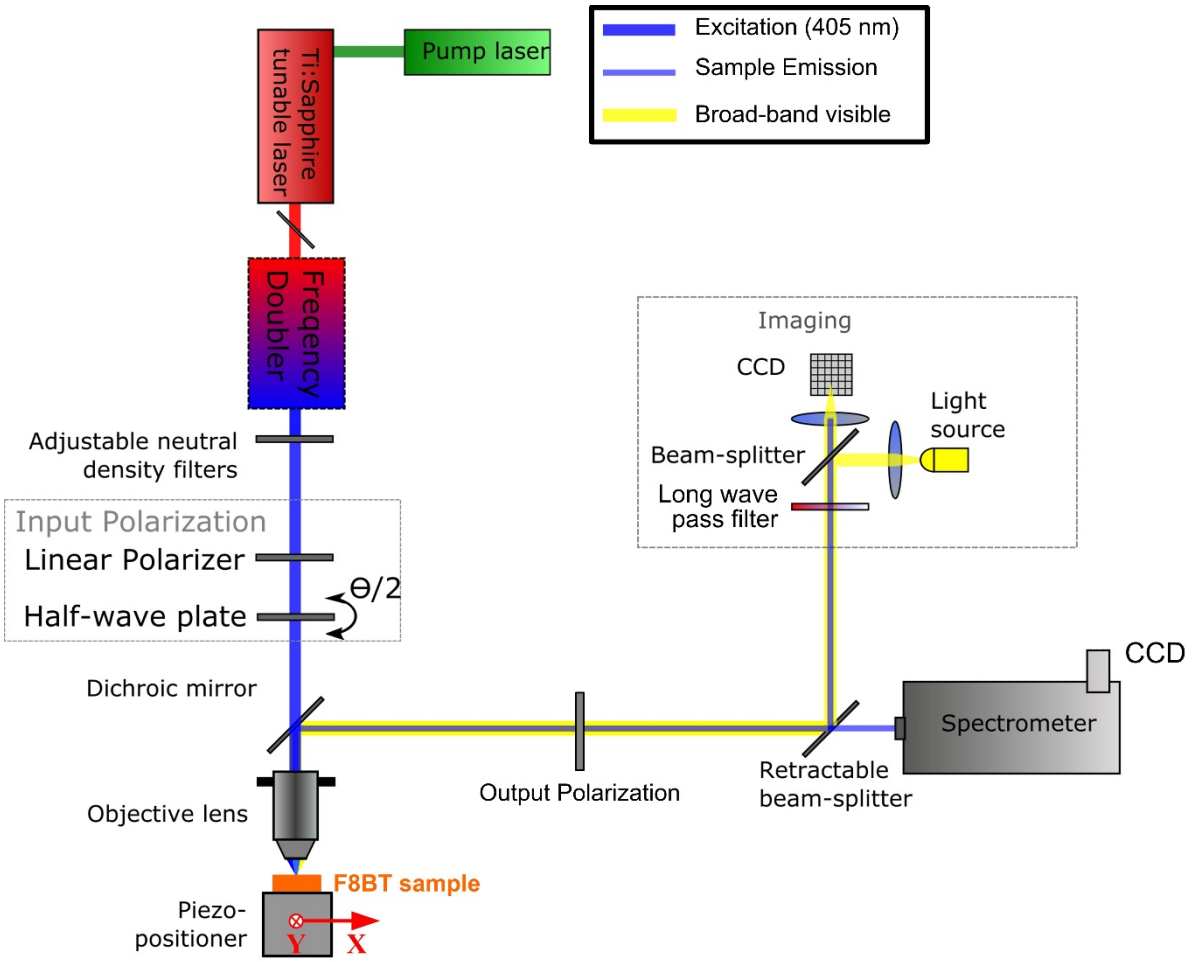

Figure S2: Experimental arrangement for mapping the micro-photoluminescence (PL) from the UV and laser aligned F8BT samples. A frequency-doubled femtosecond Ti:sapphire laser (100 fs pulses at 76 MHz) operating at 405 nm was used as the excitation source for the micro-PL measurements. The laser was focused on the top surface of a F8BT film by a 100× objective with a numerical aperture of NA = 0.7. The spot size of the incident laser beam focused on the sample was ≈ 1 μm in diameter. The polarization of the incident light and the collected PL spectra were controlled using a combination of linear polarizers and half-wave plates in front of the objective and the spectrometer, respectively. The excited PL emission was collected by the same objective, dispersed by a 0.3-m-long spectrometer with a 300 lines/mm grating and detected by a thermoelectrically cooled charge-coupled device (CCD). For alignment purposes, the sample was illuminated by a broadband visible light source (yellow path) and an image of the sample was then collected by a CCD camera. A 430 nm long pass filter was used to remove the excitation laser. For the mapping of the micro-PL spectra, the samples were held on a piezo-electric controlled platform with a scanning area of 100 μm×100 μm and scanning step size of 1μm in both directions.

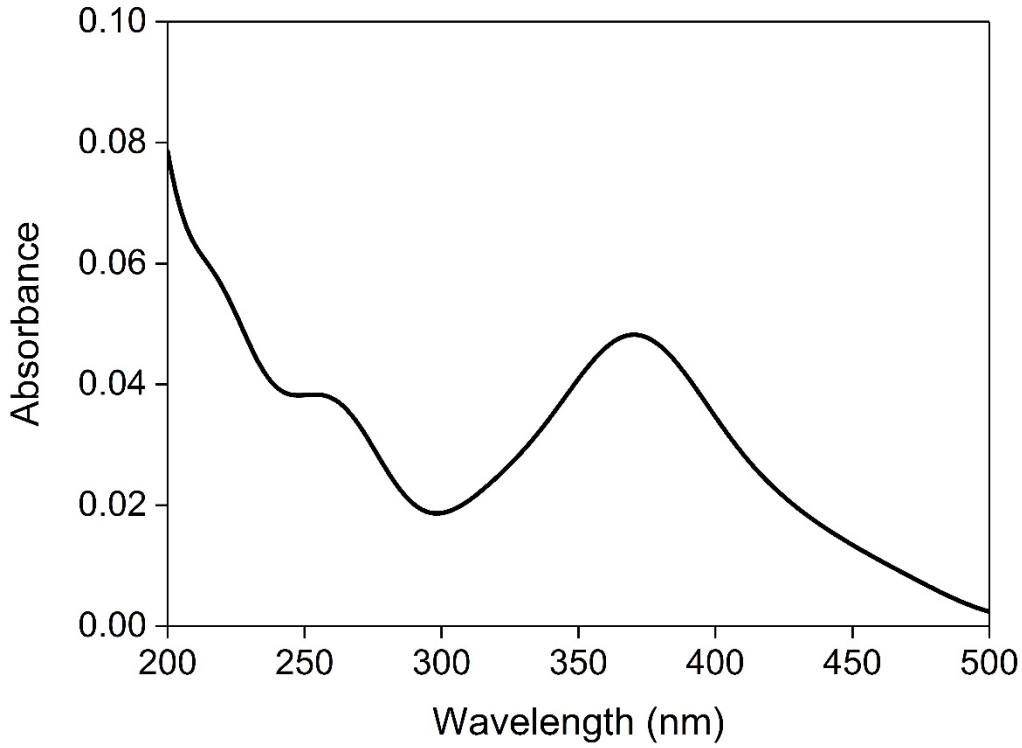

Figure S3. Absorbance spectrum for an SD1 alignment layer spin coated from a 1 mg/ml SD1 solution in anhydrous 2-methoxyethanol onto a pre-cleaned polished Spectrosil substrate at 500 rpm for 5 seconds then 2000 rpm for 20 seconds, before undergoing any photoalignment process. The long wavelength peak sits at 371 nm. UV-alignment was performed by exposure to 365 nm light from a Thorlabs CS2010 UV-curing LED system and laser (re)writing was done at 785 nm, yielding two-photon absorption at 392.5 nm; in both cases closely tuned to the long wavelength peak.

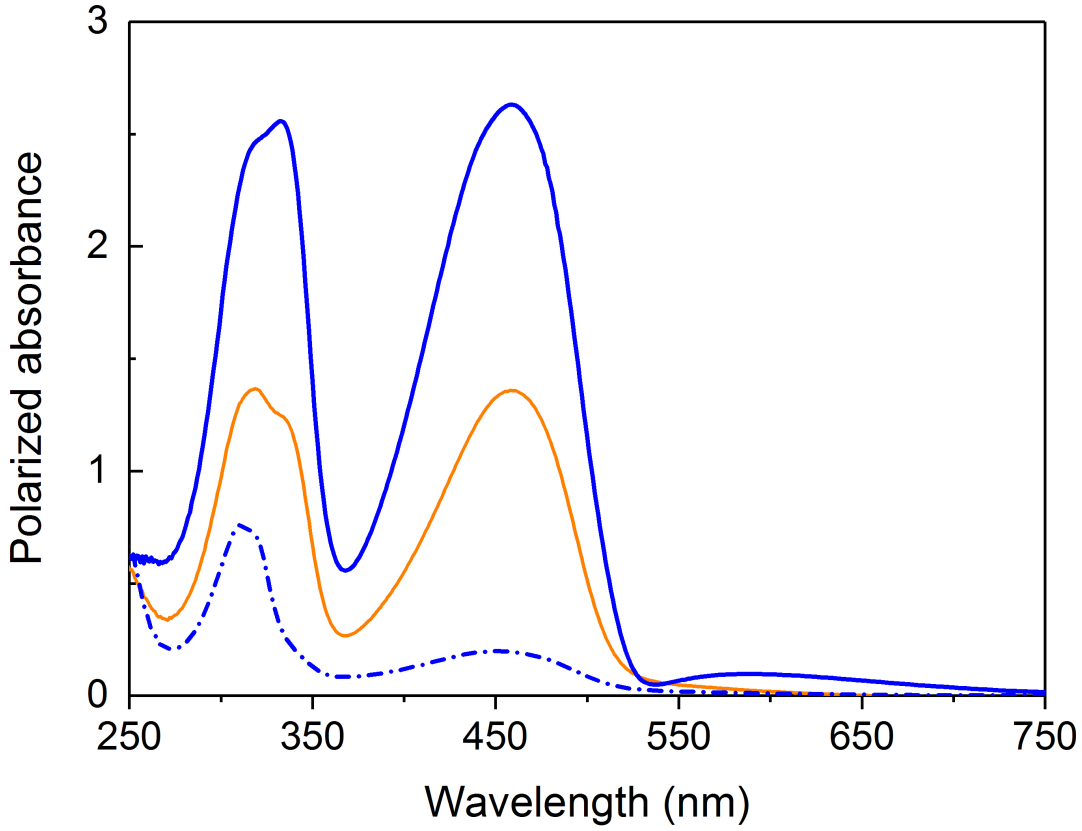

Figure S4. Polarized absorbance spectra for a F8BT film oriented on a polarized-UV-light exposed SD1 alignment layer. Spectra are shown for both parallel (solid blue line, top) and perpendicular (dashed blue line, bottom) incident polarizations, relative to the polymer chain orientation direction. Also shown (orange line, middle) is the spectrum (without incident light polarization) for a (Dektak profilometer measured) 165 ± 5 nm thickness, non-aligned F8BT film spin-coated on non-aligned SD1. This film has the same thickness as the oriented film in order to allow a direct comparison. The uniformity of the oriented F8BT film is evident from the long wavelength interference fringe seen in the parallel polarized spectrum. The dichroic ratio between the parallel and perpendicular absorption components at the long wavelength (~ 450 nm) peak was found to be 12.6 ± 0.3, which corresponds to an order parameter of $S \approx 0.85$. This value for the order parameter for an F8BT film oriented on a polarized-UV-light exposed SD1 alignment layer has been estimated based on the parallel ($A_{//}$) and perpendicular ($A_{\perp}$) components of the absorbance using $S = (A_{//} - A_{\perp}) / (A_{//} + 2 A_{\perp})$.

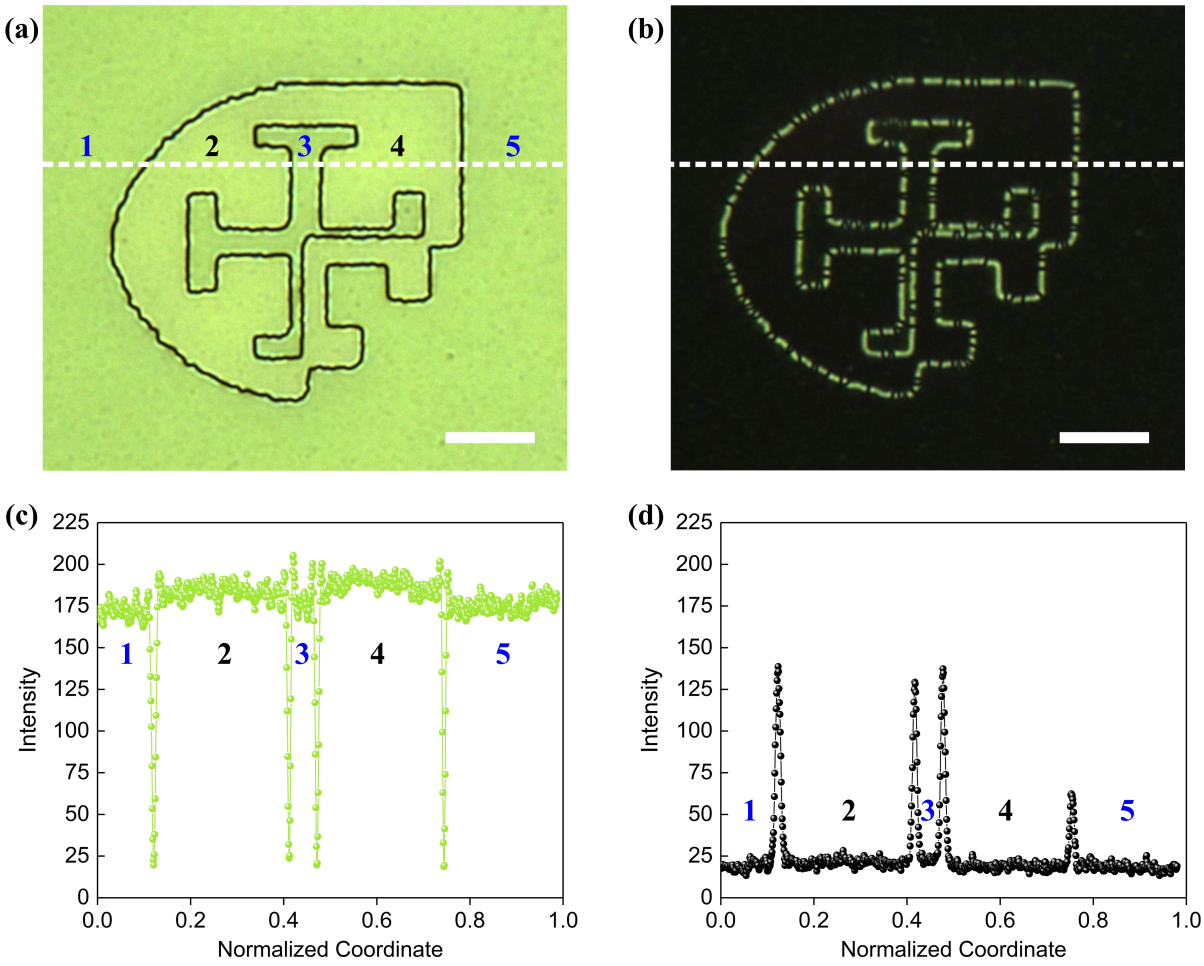

Figure S5. Comparison of the alignment of an F8BT film oriented on regions of SD1 alignment layer that have been exposed either with polarized-UV-light or with the laser writer (90°-laser-written crest). Polarized optical micrographs for the bright (a) and dark states (b) are presented along with the corresponding greyscale profiles (c) and (d), respectively, that have been extracted along the white-dashed horizontal lines in (a) and (b). Regions #1, #3 and #5 represent the UV-aligned background whereas regions #2 and #4 are for the spatially patterned crest created from laser rewriting of the SD1 alignment layer with a polarisation orientation of the laser that is at 90º to the UV-exposed regions. The white scale bars in (a - b) are 20 µm. The width of the transition zone between the laser written and UV-aligned regions was estimated to be ~1.7 - 2.5 µm. Also, we can see that the average intensity in the bright-state greyscale transmission intensity for the laser-written crest is slightly larger (by ~7% - 9%) than that for the F8BT film, oriented in regions of the SD1 alignment layer that have been exposed to polarized-UV-light. The dark-state transmitted intensities, on the other hand, are nearly identical. This would indicate a slightly larger order parameter for the F8BT film oriented on regions of the SD1 alignment layer that have been exposed to the laser writer.

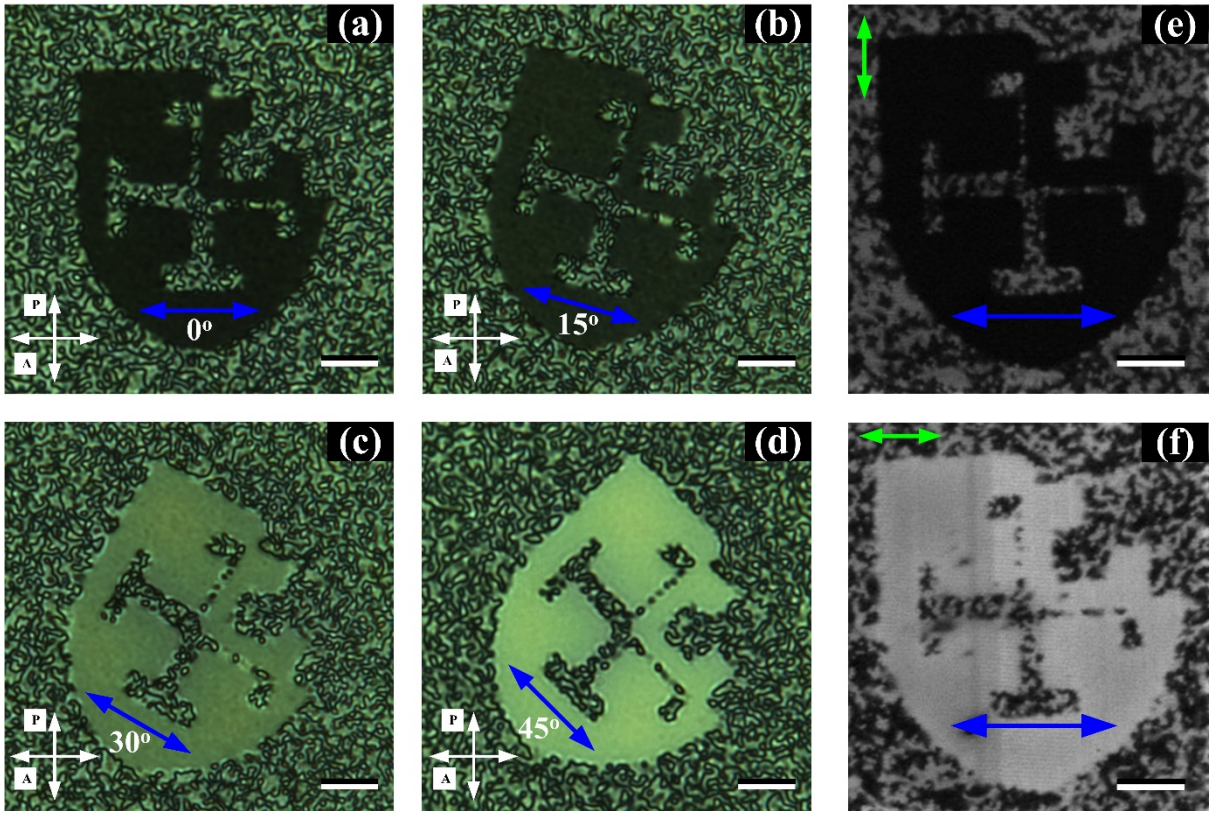

Figure S6. (a - d) Polarized optical micrographs (viewed between crossed polarizer (P, vertical doubled headed white arrow) and analyzer (A, horizontal white double headed arrow)) and (e - f) polarized PL intensity images of a laser written F8BT crest pattern. This pattern was written onto an otherwise non-aligned SD1 layer. The orientation of the F8BT polymer chains in the film (following thermotropic alignment) is indicated in each image by a double headed solid blue arrow. The numerical values next to these arrows are the angles subtended between the chain axis and the analyzer polarization direction. The polarized PL intensity images were recorded by maintaining focus on the patterned region and rotating the emission analyzer polarization direction (double headed green arrows) to be perpendicular (e) and parallel (f) to the orientation of the F8BT polymer chains in the crest pattern. For (e) and (f) the samples were excited at 450 nm with an unpolarized excitation source. The Schlieren texture evident in the background to the crest pattern is as expected for a polydomain nematic glass and contrasts with the mondomain formed by alignment within the crest pattern. The polydomain to monodomain interfacial region leads to a loss of fidelity in the pattern. The horizontal scale bar in the bottom right of each image is 20 μm in length.

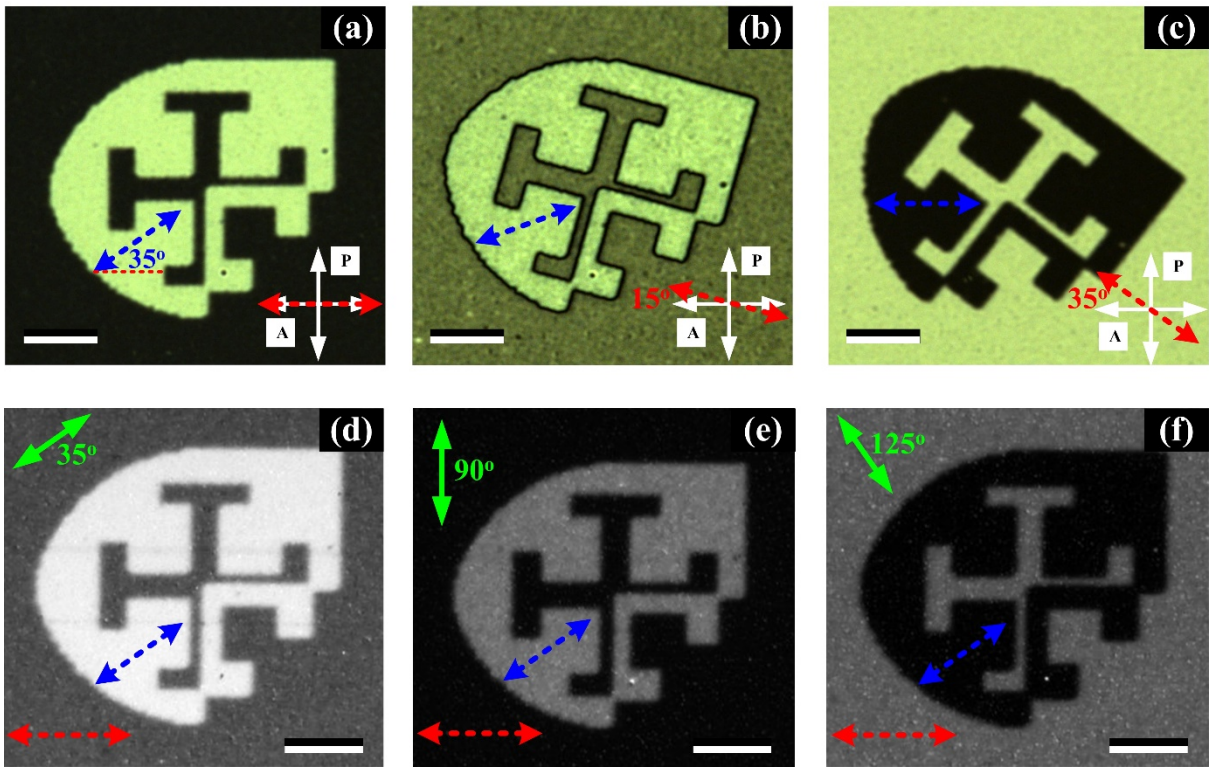

Figure S7. (a - c) Polarized optical micrographs (viewed between crossed polarizer (P, vertical doubled headed white arrow) and analyzer (A, horizontal white double headed arrow)) and (d - f) Polarized PL intensity images of a laser rewritten F8BT crest pattern. The sample preparation process involved the uniform, polarized UV-LED-exposure of the SD1 layer followed by laser writing of the crest pattern and then the F8BT film was deposited and thermally aligned on top of the SD1 layer. In this exemplar case, the orientation of the polymer chains (dashed blue doubled headed arrow) in the crest pattern is at 35° to those atop the uniformly UV-aligned SD1 background layer (dashed red doubled headed arrow). (a) A bright state of the crest and dark-state of the background, with the polarizer orthogonal to the chain orientation direction in the background; (b) An intermediate state obtained by a 15° film rotation from (a). The dark state of the pattern edges suggests a finite transition region between the crest pattern and the background; and (c) a dark-state of the crest and bright state of the background, obtained by a 35° film rotation from (a). The PL intensity images were acquired by altering the relative angle between the polarization direction (green doubled headed arrows) of an emission analyzer and the orientation of the background polymer chains (dashed red doubled headed arrow). Images (d), (e), and (f) were recorded for relative angles 35°, 90°, and 125°, corresponding to an emission collection polarization that is parallel in (d), at 55° in (e) and orthogonal in (f), respectively, to the chain alignment direction in the laser-rewritten crest (dashed blue doubled headed arrow). For images (d), (e), and (f) the samples were excited at 450 nm with an unpolarized excitation source. The horizontal scale bar in each image is 20 µm in length.

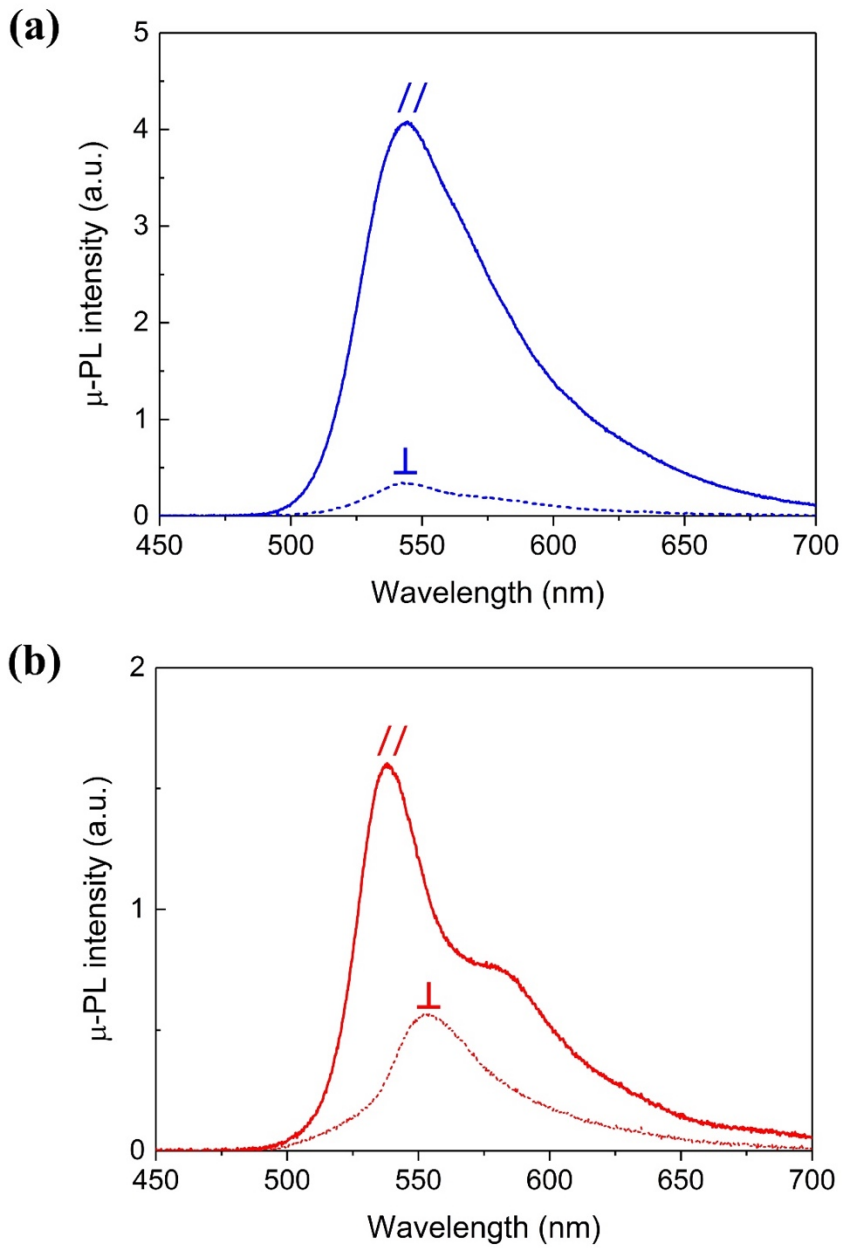

Figure S8. Micro-PL spectra for (a) an F8BT film on a UV-aligned SD1 layer and (b) an F8BT film on an SD1 layer that had been first aligned using UV illumination and then rewritten with the laser writer. In both cases, the 400 nm, 150 fs, 76 MHz, frequency-doubled Ti:sapphire laser excitation was linearly polarized orthogonal to the orientation of the polymer chains and spectra are shown for PL emission polarized both along the chain direction ($PL_{//}$) and perpendicular to it ($PL_{\perp}$). The anisotropy ratios at the peaks in their respective $PL_{//}$ spectra are 12.3 at 544 nm for (a) and 5.3 at 538 nm for (b). The $PL_{\perp}$ spectra peak at 543 nm and 554 nm, respectively, for (a) and (b).

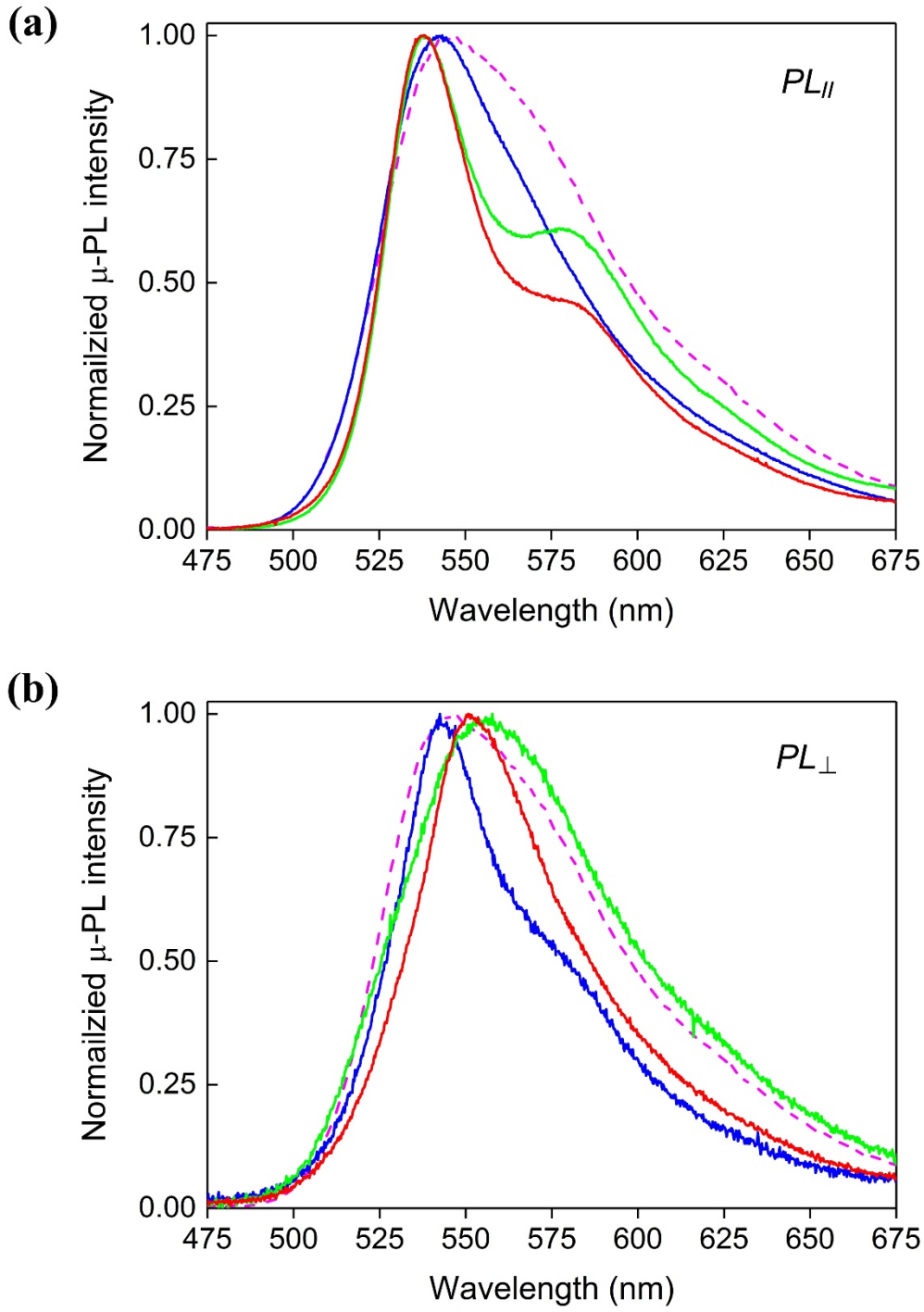

Figure S9. Peak normalized micro-PL spectra for F8BT annealed and quenched on top of a crest-pattern that was laser rewritten on a nonaligned (solid green line) and a uniformly UV aligned (solid red line) SD1 film. Also shown are the spectra for F8BT annealed and quenched on top of a non-patterned UV-aligned (solid blue line) and a non-aligned (dashed pink line) SD1 film. Spectra are shown for (a) parallel ($PL_{//}$) and (b) perpendicular ($PL_{\perp}$) polarized emission relative to the chain orientation direction. In both cases, the spectra were obtained using an excitation polarization that was parallel to the chain orientation direction.

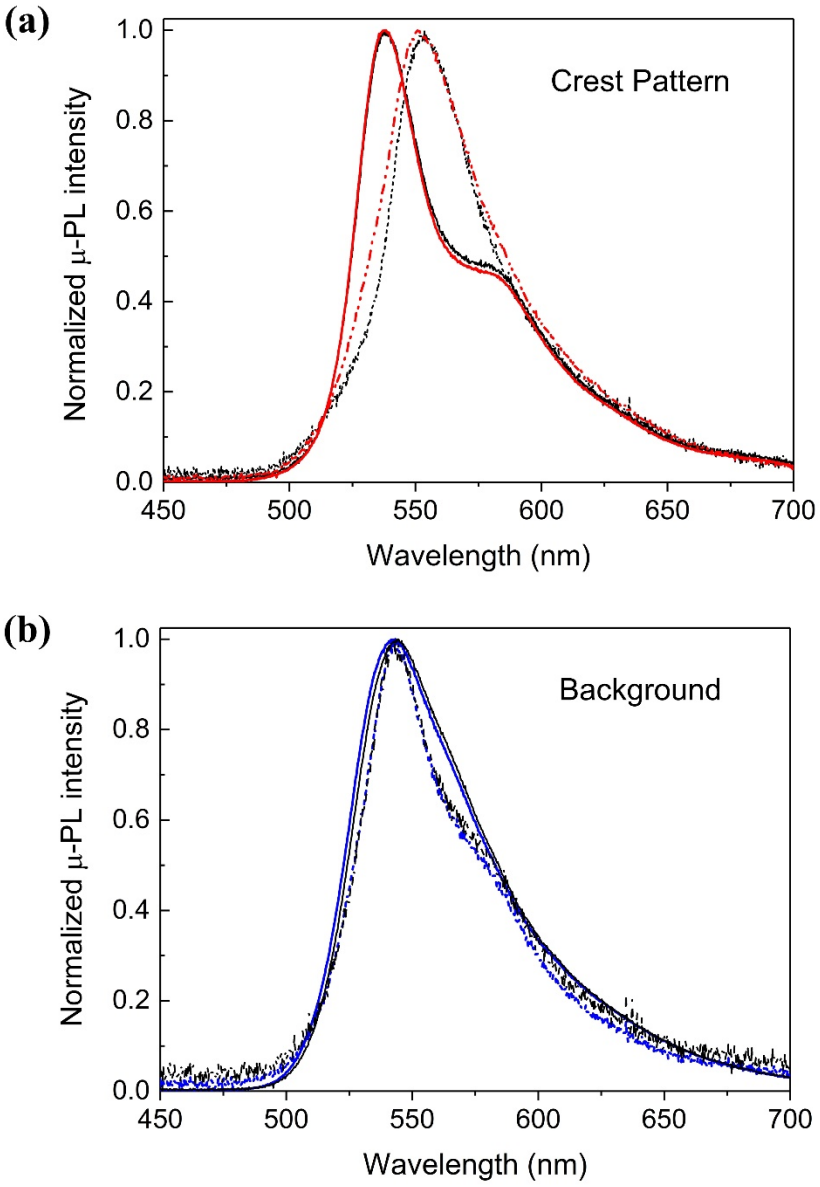

Figure S10. Peak normalized micro-PL spectra for F8BT annealed and quenched on top of aligned SD1. (a) Spectra for the SD1 crest-pattern laser rewritten at 90° on a uniformly UV-aligned SD1 background. Solid lines are for emission polarized parallel to the polymer chains, with excitation either parallel (red line) or perpendicular (black line) thereto. Dashed lines are for emission polarized orthogonal to the chain direction, with excitation either parallel (red dashed line) or perpendicular (black dashed line) thereto. (b) Spectra for the UV-aligned SD1 background. Again, solid lines are for emission parallel to the polymer chains, with excitation either parallel (blue line) or perpendicular (black line) thereto. Dashed lines are for emission orthogonal to the chain direction, with excitation either parallel (blue dashed line) or perpendicular (black dashed line) thereto.